Articles in PresS. Am J Physiol Gastrointest Liver Physiol (September 7, 2017). doi:10.1152/ajpgi.00221.2017

A physics-based model for maintenance of the pH gradient in the gastric mucus layer

Owen L. Lewis[1,†], James P. Keener[1,2], and Aaron L. Fogelson[1,2]

[1]Department of Mathematics, University of Utah
[2]Department of Bioengineering, University of Utah
[†]Corresponding Author: olewis@math.utah.edu

August 30, 2017

Abstract

It is generally accepted that the gastric mucus layer provides a protective barrier between the lumen and the mucosa, shielding the mucosa from acid and digestive enzymes and preventing auto-digestion of the stomach epithelium. However, the precise mechanisms that contribute to this protective function are still up for debate. In particular, it is not clear what physical processes are responsible for transporting hydrogen protons, secreted within the gastric pits, across the mucus layer to the lumen without acidifying the environment adjacent to the epithelium. One hypothesis is that hydrogen may be bound to the mucin polymers themselves as they are convected away from the mucosal surface and eventually degraded in the stomach lumen. It is also not clear what mechanisms prevent hydrogen from diffusing back toward the mucosal surface, thereby lowering the local pH. In this work we investigate a physics-based model of ion transport within the mucosal layer based on a Nernst-Planck-like equation. Analysis of this model shows that the mechanism of transporting protons bound to the mucus gel is capable of reproducing the trans-mucus pH gradients reported in the literature. Furthermore, when coupled with ion exchange at the epithelial surface, our analysis shows that bicarbonate secretion alone is capable of neutralizing the epithelial pH, even in the face of enormous diffusive gradients of hydrogen. Maintenance of the pH gradient is found to be robust to a wide array of perturbations in both physiological and phenomenological model parameters, suggesting a robust physiological control mechanism.

New & Noteworthy

This work combines modeling techniques based on physical principles, as well as novel numerical simulations to test the plausibility of one hypothesized mechanism for proton transport across the gastric mucus layer. Results show that this mechanism is able to maintain the extreme pH gradient seen in *in vivo* experiments and suggests a highly robust regulation mechanism to maintain this gradient in the face of dynamic lumen composition.

1 Introduction

It is generally accepted that the gastric mucus layer provides a protective barrier between the stomach lumen and the mucosa, shielding the mucosa from acid and digestive enzymes and preventing auto-digestion of the stomach epithelium. However, the precise mechanisms that contribute to this protective function have long been a source of debate, and there are numerous unanswered questions regarding the prevention of epithelial injury due to the lumenal environment. The most direct evidence of the role of gastric mucus in mucosal protection is the existence of a large pH gradient across the mucus layer. The pH of the stomach lumen is a dynamic quantity, changing as food is ingested and in response to a variety of other factors [26]. Regardless, the lumen is consistently an acidic environment, often exhibiting a pH of two or lower [4]. Decades ago, it was demonstrated that while the pH in the lumen is highly acidic, the ambient pH at the base of the mucus layer, immediately adjacent to the epithelium, is almost neutral [30, 4]. This indicates a change in hydrogen concentration of five orders of magnitude or more. Because the thickness of the mucus layer is generally on the scale of hundreds of microns, these measurements imply that the gradient of proton concentration is enormous. At this point it is still an open question how hydrogen ions, which are produced underneath the mucus layer in the gastric glands, are transported to the lumen without acidifying the environment adjacent to the epithelium. Furthermore, it is not clear why hydrogen does not readily diffuse back to the epithelium from the stomach lumen, acidifying the environment of the epithelium.

One hypothesis for how hydrogen transport is accomplished was put forth by Schreiber, et. al. [25]. A series of titration experiments using purified and whole guinea pig gastric mucus showed

that at a critical pH, whole mucus released a "burst" of hydrogen. Conversely, purified guinea pig mucus and mucus treated with pepstatin (to inhibit the function of pepsin) did not exhibit this release of hydrogen regardless of ambient pH. The resulting conclusion is that the released hydrogen must have been sequestered somewhere within the whole mucus sample, and released by the pH-dependent activation/action of pepsin. Based on these experiments, the authors hypothesized that hydrogen secreted in the gastric pit is sequestered on the gastric mucin polymers themselves. Upon reaching a critical pH threshold, pepsinogen is activated into pepsin, and begins degrading mucin polymers, thereby destroying their capacity to sequester hydrogen and releasing it into the environment.

The hypothesis of Schreiber has yet to be corroborated, and indeed there are competing thoughts as to the process by which hydrogen is transported to the lumenal side of the mucus layer. Several studies have observed acidic "channels" within the mucus layer, suggesting that localized flows of proton rich fluid transport hydrogen through the mucus. Other studies have failed to observe these channels [15, 16, 7]. As yet, no consensus has been reached, and it is unclear how to experimentally determine the validity of either hypothesized mechanism. For this reason, the topic is a prime candidate for exploration via a mathematical model. Early modeling work showed that bicarbonate secretion at the epithelial wall was capable of neutralizing the mucosal surface, when considering species diffusing according to Fick's Law. However, according to that model, the secretion of bicarbonate would need to be an order of magnitude greater than hydrogen secretion to achieve neutralization [11]. More recent investigations have suggested that bicarbonate secretion on the same scale as hydrogen secretion may be sufficient [19]. However, we know of no modeling effort that accounts for both the chemistry of bicarbonate buffering and the electro-diffusive nature of hydrogen ions, nor how these physical processes in the stomach interact with secretion at the mucosal wall.

The main goal of this work is to develop and analyze a mathematical model of the physics of ion transport within the gastric mucus layer under the assumption that Schreiber's hypothesis is correct. It is found that such a model can account for the massive pH gradient observed *in vivo*. Additionally, we find that the physical system is robust to perturbations in both phenomenological modeling parameters, as well as physiological parameters. In total, our model indicates that Schreiber's hypothesis is physically consistent with pH measurements reported in the literature, and suggests an extremely robust mechanism with which to maintain physiologically relevant pH profiles within the gastric mucus layer.

2 Mathematical Model

To mathematically represent the gastric mucus layer, we utilize a "two-phase gel" framework [27]. In this framework, at each point in space there may simultaneously exist two materials: the "gel" (meant to represent the cross-linked mucin polymer network), and the "solvent" (meant to represent the interstitial hydrating fluid). The local composition of the resulting complex material is described by the dimensionless quantities θ_g and θ_s which represent the "volume fraction" of network and solvent respectively (i.e. the fraction of local volume which is made up of each phase). Together, the two phases must fill space, and therefore $\theta_g + \theta_s = 1$. Generically, in two-phase models θ_g and θ_s may have spatial and temporal dependence, but in this work they are constant in time and their spatial profiles imposed (discussed more below).

The quantities of interest in our model are the concentration of four ionic species. Specifically, we are interested in concentrations defined as moles per volume of *solvent*, not moles per total volume (a technical, but important distinction). Hydrogen and bicarbonate are explicitly tracked

by C_H and C_B, both with units of Molar. All other cations and anions are represented by C_I and C_A, respectively, measured in units of Equivalent per liter (which we denote M for notational convenience throughout this work). For simplicity, we analyze a model in one spatial dimension. The spatial variable x measures distance from the epithelial wall of the stomach towards the lumen, and thus the location $x = 0$ corresponds to the epithelial surface. The evolution of the concentration of ionic species is governed by a Nernst-Planck type equation, which describes the flux of ions due to advection, diffusion, and the electric potential gradient, as well as any reactions and sources that impact ionic concentration. A careful derivation (see [27]) of the transport law for ionic species in a two-phase mixtures results in the following equation:

$$\frac{\partial}{\partial t}C_i + \frac{\partial}{\partial x}\Big(\underbrace{uC_i}_{\text{I}}\Big) = \frac{1}{\theta_s}\frac{\partial}{\partial x}\left(\theta_s\left(\underbrace{D_i\frac{\partial}{\partial x}C_i}_{\text{II}} + \underbrace{z_i D_i C_i \frac{\partial}{\partial x}\Psi}_{\text{III}}\right)\right) + \underbrace{f_i}_{\text{IV}}, \tag{1}$$

Here, the index i may take the values $i = H, B, A, I$ for hydrogen, bicarbonate, anions, and cations respectively. Terms I, II, and III represent changes in ionic concentration due to advective, diffusive, and electric fluxes respectively. Term IV represents any reactions and/or sources which impact the concentration of species i. The variable u is the velocity of the fluid solvent (in cm/sec) which results from secretion of fluid at the stomach wall. Though eq. (1) is valid for velocities that vary in space and time, we assume that u does not vary in time. The parameter D_i is the diffusion coefficient of species i, with units of cm^2/sec, z_i is the valence of the ith ionic species (± 1), and Ψ denotes the non-dimensional electric potential (which may be converted to voltage by multiplying by RT/F, where R is the ideal gas constant, T is absolute temperature, and F is the Faraday constant). Note that eq. (1) is similar to a standard Nernst-Planck transport equation with the exception of two appearances of θ_s on the right hand side. These terms account for the fact that the ionic species are transported within the *solvent* phase of a mixture whose composition may have spatiotemporal variations.

The electric potential Ψ does not have its own equation of state. Rather, it is determined by enforcing an electro-neutrality constraint. Ionic concentration variations are not allowed to result in a collection of net-charge at any location within the domain. Mathematically this physical constraint is expressed as

$$\sum_i z_i C_i = 0, \tag{2}$$

A detailed derivation of this modeling framework can be found in [27].

For the purposes of this work, we imagine that gastric mucus is constantly produced at the epithelial surface, moves away from the wall, and is degraded as it approaches the lumen in a manner which results in a standing front that defines the edge of the mucus layer. At this front, the degradation of mucus results in a release of hydrogen ions. We do not explicitly model the mucus phase dynamics, only their effect on dissolved ions, namely maintaining a source of hydrogen near the lumenal edge of the mucus layer. Therefore, we choose θ_g to have a spatial profile that captures the transition from the mucus gel layer to the stomach lumen; it does not change in time. Figure 1 shows the spatial form of θ_g (recall that $\theta_s = 1 - \theta_g$). Moving away from the stomach wall ($x = 0$), the volume fraction transitions from a value of 0.02 (in biogels such as mucus, the actual polymeric proteins which make up the gel generally occupy approximately 2% of the volume), to a value of 0. We define the "lumen" as the region where mucus network occupies less than 1% of the local volume. Conversely the "mucus layer" is defined by the region where mucus network occupies 1% or more of the volume. This transition occurs 500 µm away from the wall and the mucus layer is

indicated by the grey shaded region in figs. 1, 2 and 4. Conservation of solvent mass dictates that at steady state, $u\theta_s$ is a constant. Once we have chosen the spatial profile of θ_s, this constraint determines the spatial profile of u. Choosing u in this manner also ensures that eq. (1) (in the absence of sources and reactions) conserves the quantities $\theta_s C_i$, which are ionic concentrations per *total* volume.

The as-yet undiscussed terms f_i incorporate any sources or chemical reactions which may impact the four concentrations. They depend on the concentration of interest. Hydrogen is affected by the buffering reaction with bicarbonate (which proceeds according to the law of mass action). For simplicity, we assume that this reaction is non-reversible; carbon dioxide cannot react with water to form hydrogen and bicarbonate ions. This is justified due to the fact that the binding and unbinding rates of the buffering reaction (2.56×10^7 M^{-1} sec^{-1} and 11 sec^{-1} respectively) lead to a minuscule dissociation constant (4.2×10^{-7} M) [11]. Hydrogen ions are also produced by a source term ($S(x)$) at the edge of the mucus layer (spatially located in the same region where the volume fraction transitions from mucus layer to lumen). Because the gel layer is in homoestasis, the source of hydrogen is assumed to be independent of time, but localized spatially,

$$f_H = S(x) - \kappa C_H C_B. \tag{3}$$

This source term is meant to represent the hydrogen released by degradation of mucus, assuming the proton transport mechanism proposed by Schreiber in [25] is correct. Furthermore, we are assuming that secreted mucus within the layer has irreversibly bound all the hydrogen it is capable of sequestering, until this hydrogen is released via mucus degradation. Thus we do not model binding/unbinding of hydrogen to the mucus layer. Because of its phenomenological nature, $S(x)$ is constructed in the following way: we truncate a Gaussian that is centered at the edge of the lumen. Outside a narrow region (whose width roughly corresponds to the transition from $\theta_g = 0.02$ to $\theta_g = 0$), we set the source to zero. The magnitude of the profile is chosen so that the spatial integral $\int S(x)\,dx$ (which corresponds to a flux of hydrogen ions) matches approximately with reported values of hydrogen flux in the human stomach. The profile of $S(x)$ we use is shown in fig. 1 and discussed in more detail in appendix A. The concentration of bicarbonate is affected by the same hydrogen/bicarbonate buffering reaction, hence

$$f_B = -\kappa C_H C_B. \tag{4}$$

Due to electro-neutrality, whenever a hydrogen ion is released by mucus degradation at the mucus/lumen interface, a corresponding negatively charged particle must be released into the stomach. Therefore, the source term also affects the concentration of anions, so

$$f_A = S(x). \tag{5}$$

We note here that we do not make any assumptions about what precise species produces this negative charge. Whether it is a chloride ion or a negatively charged unit on a degraded mucin polymer, all negative charges (other than bicarbonate) are treated as a single species. Finally, we assume that cations are not affected by any sources or reactions, so

$$f_I = 0. \tag{6}$$

The transport law eq. (1) must be accompanied by boundary conditions at the epithelial wall and the bulk stomach lumen. For boundary conditions at the wall ($x = 0$), we impose a flux relation that depends on the local ionic concentrations at the epithelial surface. We *do not* explicitly specify

the flux of any ion through the epithelial surface. For each species, the *total* flux from the transport equation is

$$\phi_i = -D_i \frac{\partial}{\partial x} C_i - D_i z_i C_i \frac{\partial}{\partial x} \Psi + C_i u. \tag{7}$$

The three individual terms on the right hand side of this expression represent the diffusive, electric, and advective (respectively) flux of the ionic species i. The flux of each species to/from the epithelial wall must balance the flux through ion exchangers embedded in the epithelial surface. Mathematically, this is represented as

$$\phi_H|_{x=0} = k_{\mathrm{HI}} \Big(C_I - \delta_{HI} C_H \Big) \Big|_{x=0}, \tag{8}$$

$$\phi_I|_{x=0} = -k_{\mathrm{HI}} \Big(C_I - \delta_{HI} C_H \Big) \Big|_{x=0}, \tag{9}$$

$$\phi_B|_{x=0} = k_{\mathrm{BA}} \Big(C_A - \delta_{BA} C_B \Big) \Big|_{x=0}, \tag{10}$$

$$\phi_A|_{x=0} = -k_{\mathrm{BA}} \Big(C_A - \delta_{BA} C_B \Big) \Big|_{x=0}. \tag{11}$$

The terms on the right hand side represent a simplified, linear model of flux due to anti-port ion exchangers [17]. We note here that we do not model any of the ion exchange taking place within the gastric pits which controls hydrogen secretion. The process of secretion is taken as a given, and (in line with the hypothesis of Schreiber) represented in the source term $S(x)$. Here we only include ion exchange *at the epithelial surface*. Both bicarbonate/chloride exchangers and hydrogen/sodium exchangers are known to be present on the apical membrane of mammalian epithelial cells, and it is known that bicarbonate secretion is chloride dependent [1]. This model of flux across the epithelial surface is discussed at more length in appendix A. For boundary conditions at the lumen (which we define as $x = 0.2$ cm), we simply impose lumenal ionic concentrations.

$$C_H|_{x=L} = H_L, \tag{12}$$

$$C_I|_{x=L} = I_L, \tag{13}$$

$$C_B|_{x=L} = B_L, \tag{14}$$

$$C_A|_{x=L} = A_L. \tag{15}$$

$$\tag{16}$$

Here, H_L, I_L, B_L and A_L are the concentrations of hydrogen, cations, bicarbonate, and anions (respectively) in the stomach lumen.

To generate the results discussed for the remainder of this work, the model was simulated using parameter values listed in table 1. The specifics of our spatial discretization and time integration are discussed in appendix B. We are specifically interested in steady state behavior, but we simulated the entire (time dependent) set of equations. To achieve "steady state" we simulated until none of the ionic concentrations (at any point in space) change by 0.1% or more during a period of 10 seconds.

3 Results

3.1 Steady State Behavior

The model was simulated until steady state was reached with $k_{\mathrm{HI}} = k_{\mathrm{BA}} = 2 \times 10^{-4}$ cm/sec. We do not have reliable data for what values of these parameters most closely represent the stomach

in vivo. Presumably, these values should be derived from the density of ion exchangers on the epithelial surface, as well as the thermodynamics of an individual ion exchanger. In the absence of estimates for the "correct" value of these parameters, we were forced to choose a parameter set to begin analysis of the model. As we discuss later, many of the predictions of the model are insensitive to this choice. For the duration of this study, we refer to the regime where $k_{\mathrm{HI}} = k_{\mathrm{BA}} = 2 \times 10^{-4}$ cm/sec as the "base case." These parameter values are also marked with a large dot on the first panel of fig. 3

Figure 2 shows the steady state behavior of the model for the base case. The first panel shows the steady state concentrations of the four ionic species. The measured pH (calculated as $-\log_{10}(C_H)$) is 2.3 at the lumen, and nearly constant up to the edge of the mucus layer (at $x = 0.05$ cm). Across the mucus layer, the measured pH transitions from 2.3 to approximately neutral (6.47). This hydrogen profile is quantitatively similar to data reported in numerous experiments [4, 24, 30]. We emphasize here that while the pH at the stomach lumen is imposed by our boundary condition, *we do not dictate the pH at the stomach wall, nor the transition across the mucus layer*. This spatial profile of hydrogen concentration is an emergent behavior due to the transport of ions, ion exchange at the wall, and the buffering reaction. It may be regarded as a prediction of the model. This means that our model supports the plausibility of the hypothesis of proton transport originally put forward in [25]. The fact that Schreiber's hypothesis of proton transport can give rise to physiological hydrogen concentrations in a physics-based model represents a major result of this work.

The first panel of fig. 2 also shows that bicarbonate only exists (in appreciable concentrations) in a small (approx 20 to 30 µm) region immediately next to the epithelial wall. A rapid decay of bicarbonate concentration to approximately zero occurs as one moves away from the wall and bicarbonate is consumed in the buffering reaction with hydrogen. The maximum concentration of bicarbonate observed is less than that of hydrogen. While the maximum concentration of bicarbonate is 0.3 mM, hydrogen concentrations within the domain reach values up to 5 mM, more than a order of magnitude greater. Cation and anion concentrations are relatively constant throughout the domain, ranging from 32 to 40 mM (cations) and 32 to 45 mM (anions).

The second panel of fig. 2 shows the various fluxes of hydrogen within the domain at steady state. Notice that because we impose a source at the edge of the mucus layer, because additional sourcing may occur at the stomach wall (due to ion exchange), and because of the buffering reaction, the total flux of hydrogen may be non-zero at steady state. However, beyond the lumenal edge of the mucus layer, the total flux of hydrogen is approximately zero. This means that there is no net transport of hydrogen within the lumen. Together with the hydrogen profile shown in the first panel of fig. 2, this indicates that the model is capable of reproducing a gastric mucus layer in homeostasis. Within and adjacent to the mucus layer however, hydrogen transport is occurring even in steady state. The diffusive flux in the outer portion of the mucus layer (away from the epithelial surface) is relatively large and negative. This indicates a large diffusive transport of hydrogen towards the epithelium. However, the effect of this flux is attenuated by a positive (from wall to lumen) flux due to the electric potential gradient (the electric potential itself varies by approximately 0.35 mV across the width mucus layer). This implies that the charged nature of ionic hydrogen causes total flux toward the wall to be less than one would expect due to purely diffusive effects. Additionally, this diffusive flux becomes drastically smaller in magnitude close to the epithelial wall. This is due to a general decrease in hydrogen concentrations because of the buffering reaction. While it appears that there is a large-scale back-diffusion of hydrogen *towards* the wall (if one examines the lumenal portion of the mucus layer), bicarbonate buffering in the narrow layer near the epithelium prevents a large back-diffusion of hydrogen *to* the wall.

It is worth noting here that the model implies that the advective flux is negligible. This could

have been predicted *a priori* by calculating the Péclet number of the system. The Péclet number is a non-dimensional parameter that characterizes the relative importance of diffusive and advective processes within a physical system. Using the velocity of solvent, and the diffusion coefficient of a hydrogen ion in water as listed in table 1, as well as a length scale of the thickness of the mucus layer ($L = 0.05$ cm) we calculate the Péclet number as

$$\mathrm{Pe} = \frac{Lu}{D_H} \approx 1.2 \times 10^{-2}.$$

A Péclet number this small indicates that diffusive transport is roughly 100 times more important than advective transport within the mucus layer, a conclusion corroborated by the results of our simulation. This directly contradicts certain hypotheses in the literature that back diffusion is counteracted by advective transport away from the wall [10]. To effectively retard back diffusion, characteristic solvent flow velocities would need to be two or more orders of magnitude larger.

3.2 Insensitivity to Ion Exchange Rate

We now return to discuss the ion exchange rate parameters k_{HI} and k_{BA}. As previously mentioned, from available experiments and literature we are unable to determine the "correct" values of these parameters that most closely represent *in vivo* conditions. The previous section shows that the model is capable of reproducing concentrations which resemble those observed in mammalian stomachs, but the question remains: do these results depend on our choice of ion exchange rates? To address this question, we simulated the model to steady state for numerous different parameter sets. We varied both k_{HI} and k_{BA} from 10^{-6} to 10^{-1} cm/sec. Once the simulation reached steady state, we measured the resulting pH at the wall. Figure 3 shows a filled contour plot of the wall pH predicted by the model as a function of both ion exchange rate parameters. The plot was generated using 256 individual data points, spaced approximately equally on a log scale. The solid black line indicates the collection of parameter values that result in a wall pH of 6. Whenever a simulation resulted in a wall pH between 6 and 8, we identify the epithelial surface as "adequately neutralized." All exchange rate values above and to the right of this solid line are adequately neutralized.

This exploration suggests that wall pH does not depend strongly on either exchanger rate. The wall is adequately neutralized for values ranging over nearly 3 orders of magnitude (for either exchanger rate). Furthermore, all simulations performed resulted in a wall pH between 4.2 and 6.8, even varying these parameters over 5 orders of magnitude. Less systematic numerical explorations indicate that varying the exchange rates further does not change this behavior. The only exception to this rule is taking one exchange rate to zero (discussed in more detail in section 3.4). Wall pH appears to approach asymptotic values for both "fast" bicarbonate exchange (large k_{BA}) and "slow" bicarbonate exchange (small k_{BA}). Obviously, if k_{BA} is set to zero, there is no bicarbonate secretion and, since there are no other sources of bicarbonate, the entire domain (including the epithelial wall) will be approximately the imposed lumenal pH.

Two examples of this asymptotic behavior can be seen in the second panel of panel of fig. 3. The two graphs show wall pH as a function of k_{BA} when k_{HI} is equal to 2×10^{-4} and 2×10^{-6} cm/sec respectively. The two dash-dot lines in the first panel of fig. 3 indicate the range of parameters used to generate these two graphs. The shaded gray region indicates wall pH values which are adequately neutralized. For both values of k_{HI} the wall pH asymptotic values lie between 4.5 and 6.7, suggesting that altering the rate of exchange of ions at the epithelial wall can affect the wall pH by less than 2.5 *even in extreme cases*. Regardless, the parameter ranges which produce wall pH measurements above 6 are still enormous. Taken together, these results have profound implications. Assuming the hydrogen transport hypothesis of Schreiber, the precise regulation of

ion exchange at the epithelial wall is not necessary to maintain the gastric pH gradient. As long as ions are exchanged "fast enough" (for a very loose definition of "fast enough"), neutralization of the stomach wall is possible and homeostasis is preserved.

This is encouraging for several reasons. Our simplified model of ion exchange assumes a constant exchange rate. A more complex model such as that in [17] would incorporate a non-linear dependence on local ionic concentrations. However, this would be unlikely to change our results, as steady state pH is unaffected by varying either parameter's value over vast ranges. Furthermore, relating the values of these parameters to "correct" values obtained from experimentally measurable quantities is difficult, but our model indicates that precisely controlled parameter values are irrelevant to the main result.

Finally, we note that in the case of very fast bicarbonate exchange (large k_{BA}), the qualitative character of the steady state ion concentrations changes somewhat. For these simulations, hydrogen concentration is no longer monotonic; there is an over neutralized alkaline region occurring within the mucus layer. This behavior appears for k_{BA} values of 5×10^{-4} cm/sec or greater, regardless of the value of k_{HI}. This transition is marked in the first panel of fig. 3 by the dashed line. All simulations to the right of this transition exhibit localized minima of hydrogen concentration within the mucus layer. As an example of this behavior, fig. 4 shows the steady state concentration of ions and flux of hydrogen predicted when $k_{\mathrm{HI}} = 1 \times 10^{-1}$ cm/sec and $k_{\mathrm{BA}} = 5 \times 10^{-4}$ cm/sec. To more clearly display near wall features, the insets show the same data between $x = 0$ and $x = 0.025$ cm. Some care should be taken when interpreting the quantitative prediction of the model near the local minima of hydrogen, as our model does not take into account the auto-ionization of water. One may reasonably assume that this effect becomes relevant whenever pH is below 7 and the rate of hydrogen production due to ionization is of a comparable scale as hydrogen removal due to the bicarbonate buffering reaction. Using the bicarbonate buffering rate κ listed in table 1, 1.3×10^{-5} sec^{-1} as the ionization rate of water, and 55.5 M as the concentration of water ([28]), a rough calculation indicates that this is true whenever the product of hydrogen and bicarbonate concentrations satisfies $C_H C_B \leq 5 \times 10^{-11}$ M^2. It is worth noting that even for parameter values that generate local minima, the steady state pH *at the wall* remains approximately neutral. This is due to the response of the hydrogen/cation exchange. Fast bicarbonate exchange can result in a large flux of bicarbonate into the domain from the epithelial wall, which tends to over-neutralize hydrogen. Coincident with this phenomenon, the flux of hydrogen through the epithelial wall *changes direction*; hydrogen is secreted at the epithelial wall. This can be seen in the second panel of fig. 4, as the total flux of hydrogen at the epithelial wall is slightly positive (in contrast to the data in the second panel of fig. 2). This source of hydrogen at the wall maintains an approximately neutral pH at that location. As hydrogen and bicarbonate diffuse away from the wall, the buffering reaction takes place, leading to a minimum in hydrogen concentration approximately 20 µm away from the epithelium. Further from the wall, hydrogen diffusing from the source at the edge of the mucus layer becomes more prevalent, eventually overcoming the bicarbonate secreted at the epithelium and lowering the local pH. In later sections we again see that the robustness of the model predictions depends on the existence of hydrogen/cation exchange and the ability of the hydrogen flux at the epithelial wall to change sign.

3.3 Insensitivity to Lumenal pH

In the modeling framework used here, we have made the assumption that the ionic composition of the stomach is fixed and can be described by four constants (H_L, I_L, B_L and A_L). Even under the assumption that the contents of the stomach are "well mixed", the ionic composition of the stomach lumen *in vivo* is unlikely to remain constant in time. For this reason, we now describe a set

of experiments that ascertain how robust the results of the model are with respect to perturbations in the luminal pH value imposed at $x = 0.2$. We performed a series of simulations where H_L is changed to reflect a desired lumenal pH. To satisfy the electro-neutrality constraint, A_L is also changed to satisfy the equation

$$A_L = H_L + I_L - B_L.$$

Lumenal concentrations of bicarbonate and cations are not altered. All simulations are performed with "base case" exchange rates ($k_{\mathrm{HI}} = k_{\mathrm{BA}} = 2 \times 10^{-4}$ cm/sec). Figure 5 shows results obtained by allowing the model to reach steady state for various values of lumenal pH.

The first panel of fig. 5 shows the measured pH at the epithelial wall as a function of the pH at the stomach lumen. The most striking feature of the graph is that while we varied lumenal pH from 1.5 to 3, we observed relatively small changes in wall pH (from approximately 6.15 to 6.5). The effect of lumenal pH changes on the wall is drastically attenuated. The system effectively suppresses the ability of the stomach wall to "feel" changes in lumenal acidity. Perhaps the second most striking feature of this graph is that wall pH is not necessarily positively correlated with lumenal pH. This means that in certain regimes, lowering the pH of the stomach lumen actually results in a more neutralized wall. At first glance, this seems counter intuitive. However, the model results provide a mechanistic explanation for this behavior which we outline below.

The second panel of fig. 5 shows the steady state flux of both hydrogen and bicarbonate through the epithelial wall (due to the ion exchangers) as a function of the pH imposed at the lumen. For reference it also shows the total flux of hydrogen due to the source imposed at the edge of the mucus layer. The solid black curve depicting the steady state secretion of bicarbonate shows a negative correlation with lumenal pH and helps explain the potential for an inverse relationship between lumenal and wall pH seen in the first panel. Lumenal pH may impact measured pH at the wall in two different ways. The first, and more obvious mechanism is that increasing the lumenal pH simply results in fewer hydrogen ions within the domain, thereby increasing the pH at the wall. However, increasing the lumenal pH may affect wall pH indirectly through bicarbonate exchange. Any decrease in lumenal hydrogen concentration is accompanied by an identical decrease in anion concentration (due to the electro-neutrality constraint). Anion concentration does not vary much between the lumen and epithelial wall (see fig. 2). This results in decreased bicarbonate/anion exchange, decreasing the flux of secreted bicarbonate at the wall. The potential result of this is an increase in hydrogen concentration (decrease in pH) at the wall, as the amount of buffering is suppressed. From the local maxima in the first panel of fig. 5, it appears that this indirect effect is secondary at lower lumenal pH values. In this regime, the decrease in total hydrogen within the domain due to raising lumenal pH has more effect on wall pH than does the impact through bicarbonate secretion via anion variations. However, the indirect impact through supressed bicarbonate exchange becomes relevant at approximately a pH of 2.5. The relative importance of the two ways lumenal pH may effect wall pH is, in part, determined by the parameter values chosen for the ion exchange model (both k's and δ's). Regardless, in all our numerical experiments, the competition of these two processes leads to variations in wall pH that are much smaller than imposed variations in lumenal pH.

Further examining the second panel of fig. 5, it is noteworthy that for lumenal pH values greater than approximately 2, the flux of bicarbonate through the wall is much greater in magnitude than hydrogen flux through the wall (an order of magnitude or more). This means that while the epithelium is secreting large amounts of bicarbonate for the buffering reaction, relatively small amounts of hydrogen cross the epithelial surface. This observation says nothing about the amount of hydrogen being sourced at the edge of the mucus layer, which we have assumed was bound to the mucus itself after being secreted within the gastric pits. The flux of bicarbonate is positive in all cases,

which means that bicarbonate is being secreted *into* the domain. Conversely, the flux of hydrogen across the epithelial wall may change sign (as we previously noted in section 3.2). This means that in the case of an extremely acidic lumen, the ion exchange model may be secreting *or removing* hydrogen at the epithelial wall at steady state. This result qualitatively agrees with experiments that show epithelial cells may absorb hydrogen from the lumen into their intracellular fluid under extremely acidic conditions [12]. Furthermore, the adaptability of hydrogen exchange is important in explaining the ability of the system to attenuate the effect that lumenal perturbations have at the wall. We discuss this more below. Finally, we point out that net hydrogen secretion (through the epithelial surface, in addition to sourced from mucus) may be greater than (at higher lumenal pH) or less than (at low lumenal pH) net bicarbonate secretion. Again, this agrees qualitatively with previous studies that show the mucosa may change from net acid to net alkaline secretion in response to lumenal pH [8].

3.4 Perturbations to lumen salt and the role of dual exchange

Here, we investigate the response of the system to perturbations in the other ionic concentrations in the stomach lumen. Again, we do this by altering the value of ionic species which appear in the boundary condition at $x = 0.2$ cm. Up to this point, lumenal concentrations of cations have been given by $I_L = 40$ mM. We now examine the steady state wall pH for two new parameter sets, one where $I_L = 60$ mM, and one where $I_L = 20$ mM. In each case, we again adjust the lumenal concentration of anions to preserve electro-neutrality. Intuitively, this can be thought of as adding (or removing) 20 mM of salt (NaCl) to the stomach lumen. We refer to the parameter sets where $I_L = 20, 40$, and 60 mM as the low, medium, and high salt stomachs. All simulations are performed with $k_{\mathrm{HI}} = 2 \times 10^{-4}$ cm/sec (as in the base case), however we simulate the low, medium, and high salt stomachs over a range of values for k_{BA}. Again, the model is run to steady state with the perturbed boundary conditions and we measure the pH at the stomach wall once the model has reached steady state.

The first panel of fig. 6 shows the steady state pH of the stomach wall as a function of k_{BA}, for all three "salt values." The grey windowed region is again meant to indicate pH values between 6 and 8. We see that the wall pH is insensitive to the rate of bicarbonate/anion exchange (there is little variation within each individual curve). All parameter values result in a wall which is adequately neutralized. Additionally, we see that the wall pH appears insensitive to lumenal salt concentrations (the three curves are similar to each other). Large changes in ionic concentrations at the stomach lumen (cation concentrations change by 100% or more between the 3 salt values) do not appreciably affect the pH measured at the wall. From high to low salt stomachs, the measured wall pH varies by less than 0.5. Taken together with the results of section 3.3, the model suggests an extremely robust mechanism for the maintenance of the gastric pH gradient.

Next, we explore the role that hydrogen/cation exchange plays in the maintenance of the pH gradient. Bicarbonate is secreted with the "purpose" of buffering hydrogen before it comes into contact with the epithelial surface. However, bicarbonate is *not* secreted in response to hydrogen, it is secreted in response to chloride (represented as generic anions in our model). It is not immediately clear what the purpose of the additional hydrogen/cation exchange is in this regulatory mechanism. We now repeat the previous experiments of the the high, medium, and low salt stomachs, but with hydrogen/cation exchange turned "off" (by setting $k_{\mathrm{HI}} = 0$). The results are shown in the second panel of fig. 6.

Immediately apparent is the fact that the insensitivity observed in the first panel is destroyed. Now, neutralization of the stomach wall is highly dependent on the ionic concentration within the lumen (the three curves are quite different from one another), and the measured wall pH may vary

drastically. Physiologically, this implies that the pH at the epithelial wall would not be maintained as the ionic composition of the stomach lumen varies due to meals, etc. Furthermore, we see that robustness with respect to the bicarbonate exchange rate is also lost when hydrogen exchange is shut off (each individual curve may vary drastically). Depending on the salt composition of the stomach, the model predicts wall pH values ranging as low as 1.8 and as high as 16, with slow bicarbonate exchange failing to neutralize the wall and fast bicarbonate exchange over-buffering the near-wall environment and leading to an alkaline environment. We note here that these predictions imply hydrogen concentrations on the order of 10^{-16} M. Again, at concentrations this low, it is likely that the ionization of interstitial water within the mucus becomes a relevant effect that our model does not take into account. For this reason, pH values this high should not be regarded as quantitatively predictive. Regardless, it is fair to say that the model predicts an overly neutralized and alkaline epithelial wall. This strongly suggests that hydrogen/cation exchange serves an important physiological purpose, even though these ions are secreted/exchanged at significantly lower rates than bicarbonate. It indicates that when hydrogen/cation exchange is absent, wall pH has an extremely sensitive dependence on bicarbonate exchange rate. Therefore, to adequately neutralize the wall, the bicarbonate exchange rate must be carefully maintained. Clearly, such a scenario necessitates a very precise mechanism to regulate the rate of bicarbonate exchange, and the failure of such a regulatory mechanism would have disastrous physiological consequences.

4 Discussion

In all, the modeling investigation undertaken here strongly indicates that Schreiber's hypothesis of proton transport, when combined with ion exchange at the epithelial wall, is capable of producing and maintaining pH gradients observed *in vivo* and *in vitro*. Release of hydrogen at the edge of the mucus layer is compatible with a physics-based model of ion transport and available data on ionic concentrations in the mucus layer. The mechanism appears robust to large perturbations in both physical and phenomenological parameters within the model. However, this robustness hinges critically on the existence of two forms of ion exchange at the epithelial wall. The secretion of bicarbonate in response to chloride is not (in itself) capable of robustly maintaining a neutral pH near the stomach wall. Indeed, without hydrogen/sodium exchange, parameters must be precisely chosen to correctly neutralize the epithelium. This hints at an important physiological function of hydrogen/sodium exchangers seen in epithelial cells. Even though our model suggests flux through such channels is small for conditions which mimic "homeostatsis", it never-the-less is vitally important to the robustness of results. Without hydrogen/sodium exchange, the system is incapable of maintaining epithelial pH in the face of changes to lumenal ionic concentration, or bicarbonate/chloride exchange rate. It is known that lumenal ionic composition is a dynamic quantity *in vivo*. However, as epithelial cells are often exfoliated from the mucosa and replaced by mucus neck cells, it stands to reason that the total number of ion exchangers in the epithelium (and thus the overall effective exchange rate) would be a dynamic quantity as well [6]. Therefore, robustness to perturbations in these quantities seems to be a necessity for any physiologically relevant control mechanism.

Finally, we note that our model predicts that the epithelial wall can be neutralized with a flux of bicarbonate (due to secretion) which is approximately equal to the flux of secreted hydrogen (in our model, represented as $S(x)$). This is in contrast to early results of modeling hydrogen buffering in gastric mucus, which suggested that a bicarbonate flux nearly ten times larger than the hydrogen flux is required to neutralize the wall [11]. Indeed, this result of our model is in line with a more recent modeling effort which suggested that the bicarbonate and hydrogen fluxes

should be of approximately the same scale [19]. However, numerous experiments have indicated that bicarbonate secretion is significantly smaller than hydrogen secretion in the stomach [21]. The results presented here do no provide a resolution to this apparent paradox.

Indeed, experimental evidence of the relatively small amount of bicarbonate secreted appears to be incompatible with conservation of mass and a steady state analysis. Any physical description of the dynamics of bicarbonate and hydrogen ions within the system can be written in the form of a continuity equation (derived from the conservation of mass):

$$\frac{\partial}{\partial t}\overline{C}_i = -\frac{\partial}{\partial x}\overline{\phi}_i + \overline{S}_i(x) - f_{\text{buffering}}. \tag{17}$$

Here, $\overline{C}_i$ denotes concentration of the ion i measure in moles *per unit total volume*, $\overline{\phi}_i$ is the flux of ion i, $\overline{S}_i$ is the function describing any sources of ion i, and $f_{\text{buffering}}$ is the rate of change of $\overline{C}_i$ due to the buffering reaction. Note, that we can arrive at this relation by multiplying eq. (1) (for $i = \text{H}, \text{B}$) by θ_s (to convert from concentrations per solvent volume to concentrations per total volume) and defining $\overline{C}_i = \theta_s C_i$, $\overline{\phi}_i = \theta_s \phi_i$, $\overline{S}_\text{H} = \theta_s S(x)$, and $f_{\text{buffering}} = \theta_s \kappa C_\text{H} C_\text{B}$. However, this expression is much more general, in that is makes no assumptions about what physical processes contribute to the fluxes of ions ($\overline{\phi}_i$), nor is it specific to the two-phase modeling framework we have adopted in this work. Subtracting eq. (17) for $i = \text{B}$ from the same equation for $i = \text{H}$, integrating with respect to space from the wall to the lumen, and assuming steady state (all time derivatives are zero) yields the expression

$$\overline{\phi}_\text{H}\big|_{x=\text{wall}} - \overline{\phi}_\text{H}\big|_{x=\text{lumen}} + \int_{\text{wall}}^{\text{lumen}} \overline{S}_\text{H}(x)\,dx = \overline{\phi}_\text{B}\big|_{x=\text{wall}} - \overline{\phi}_\text{B}\big|_{x=\text{lumen}} + \int_{\text{wall}}^{\text{lumen}} \overline{S}_\text{B}(x)\,dx.$$

Now, if we assume (as all modeling work we are familiar with does) that there are no sources of bicarbonate within the domain ($\overline{S}_\text{B}(x) = 0$), and that there is no flux of bicarbonate at the lumen ($\overline{\phi}_\text{B}\big|_{x=\text{lumen}} = 0$) because bicarbonate concentrations are essentially non-existent there, we arrive a the following conclusion

$$\overline{\phi}_\text{H}\big|_{x=\text{wall}} + \int_{\text{wall}}^{\text{lumen}} \overline{S}_\text{H}(x)\,dx - \overline{\phi}_\text{H}\big|_{x=\text{lumen}} = \overline{\phi}_\text{B}\big|_{x=\text{wall}}.$$

This relationship may be interpreted to say that the flux of bicarbonate secreted at the stomach wall must balance the *net* hydrogen secreted into the stomach. This result, while consistent with the conclusions of the modeling work done here, appears to directly contradict the notion that bicarbonate secretion is an order of magnitude smaller than hydrogen secretion. It is possible that this disagreement is due to difficulties in accurately measuring secretion at the epithelium (as opposed to secreted juice which makes its way across the mucus layer after some buffering has occured). It is also possible that modeling efforts up to now have failed to account for some "sink" of hydrogen within the stomach, possibly due to drainage from the stomach lumen through the pylorus. This idea warrants further investigation and may prove useful in reconciling the apparent discrepancy between theoretical and experimental results.

Acknowledgements The work here was partially supported by NSF grant DMS-1148230 (supporting O. Lewis and J. Keener), as well as NSF grant DMS-1160432 (supporting A. Fogelson and J. Keener).

Appendices

A Parameter Estimation

Diffusion Coefficients Precisely measuring the diffusion coefficient of ionic species in solution is a difficult problem. The "effective" diffusion coefficient for dissolved ions are known to depend on ambient temperature. Furthermore, it is difficult to distinguish between transport caused by concentration gradients, and transport due to electric effects. It is also known that the effective diffusion of hydrogen in mucus is approximately four times slower than in aqueous solution [29]. However, because our model explicitly treats flux due to interactions with the electric potential as a separate term, and because we explicitly account for the effects that mucus gel has on ionic transport due to volume occlusion, we would like to use ionic diffusion coefficients which account only for Fickian diffusion. Standard estimates for the diffusivity of hydrogen ions can range between 9×10^{-5} cm^2/sec [14] and 4.5×10^{-5} cm^2/sec [9]. Because the standard estimate is for aqueous solutions at 25°C (approximately 12°C below body temperature), and because it likely does not distinguish between Fickian and electro-diffusive effects, we choose to use value on the upper end of this range ($D_{\mathrm{H}} = 7 \times 10^{-5}$ cm^2/sec). Data on the value of D_{B} is less prevalent, however molecular dynamics simulations that interpolate the limited experimental data have suggested that it should lie between 1.5×10^{-5} and 2×10^{-5} cm^2/sec at body temperature [31]. For our purposes, we choose a value of $D_{\mathrm{B}} = 1.75 \times 10^{-5}$ cm^2/sec, as it lies in the middle of this range. The "correct" values of D_{A} and D_{I} are less clear. In our model, these parameters quantify the diffusivity of the aggregate anion and cation species respectively. Though other ions clearly exist within the stomach lumen, the components of C_{A} and C_{I} which are most critical to our model are chloride and sodium (as they control ion exchange at the wall). Therefore we wish D_{A} and D_{I} to at least approximate the diffusivity of chloride and sodium. Standard tables list the diffusion coefficient of sodium and chloride as 1.3 and 2.0×10^{-5} cm^2/sec respectively [14]. However, these values are for solutions at 25°C, and are unlikely to distinguish between Fickian and electro-diffusion. Furthermore, we find it unlikely that the diffusion of small monatomic ions such as sodium and chloride would be no faster than that of bicarbonate. For this reason we choose $D_{\mathrm{A}} = D_{\mathrm{I}} = 2.5 \times 10^{-5}$ cm^2/sec. These values are also approximately consistent with what one would calculate using our listed value of D_{H}, assuming that all ionic species are spheres of constant density (with mass proportional to radius cubed) diffusing according to a Stokes-Einstein relation (diffusion coefficient scaling as the inverse of radius).

Solvent Velocity In the two phase gel modeling framework, the quantity $\theta_g u_g + \theta_s u_s$, evaluated at the stomach wall represents a flux of total volume being secreted by the mucosa (here u_g and u_s are the velocity of the gel and solvent phases respectively). For the purposes of this work, we assume that both mucus gel and interstitial fluid are secreted at the same velocity u. In [25], the authors measure the growth rate of the mucus layer produced by freshly excised guinea pig mucosa. In the case of a mucosa stimulated with histamine, the *outer edge* of the mucus layer was observed to grow at a rate of $1.25 \pm 0.33 \times 10^{-5}$ cm/sec. Conservation of total volume implies that this value must also be the flux of volume secreted at the mucosal wall, and our assumption that gel and solvent move with the same velocity implies that our solvent velocity should match the measurements given in [25]. Because we wanted our investigation to account for any potential effects that advective flux may have on ionic gradients, we chose a value of $u\theta_s$ consistent with the very largest limit of the numbers reported in [25].

Lumenal Concentrations We arrived at the value of H_L listed in table 1 through numerical experimentation. This was the lumenal hydrogen concentration which resulted in zero net flux through the lumenal boundary of our computational domain. This concentration corresponds to a lumenal pH of 2.3, which is well in the range of observed pH within the gastric lumen [6]. Many classical studies on the ionic makeup of the stomach measure the composition of gastric juice secreted into an empty stomach [23]. These studies report cation concentrations on the order of 100 mM or more. However, during the course of the day, the gastric lumen is likely to be often filled with food and various liquids which may dilute the ionic concentrations therein. Studies conducted on human patients have shown that 90 minutes after a meal, the concentration of cations within the stomach may be closer to 50 mM [13]. For this reason, we choose $I_L = 40$ mM as our standard ionic concentration and perturb the parameter about this value for the experiments of section 3.4. All studies cited above indicate that bicarbonate concentrations in the lumen are negligible. For this reason we choose $B_L = 2.2 \times 10^{-16}$ M. Finally, in all simulations and experiments, A_L is chosen to satisfy the principle of electro-neutrality.

Ion Exchanger Offsets A linearized version of an anti-port ion exchanger for bicarbonate and chloride can be written in terms of the concentrations of bicarbonate and chloride on either side of the epithelial cell membrane

$$\phi_{\mathrm{B}} = \tilde{k}_{\mathrm{BA}} \left([\mathrm{Cl}]_{\mathrm{wall}} [\mathrm{B}]_{\mathrm{cell}} - [\mathrm{Cl}]_{\mathrm{cell}} [\mathrm{B}]_{\mathrm{wall}} \right). \tag{A.1}$$

Here, the subscript "wall" refers to the concentration of the ionic species at the lumenal side of the epithelial cell wall, and the subscript "cell" refers to intracellular concentrations. A detailed derivation of a more complicated model may be found in [17]. In general, the parameter $\tilde{k}_{BA}$ has a functional dependence on the given ionic concentrations. As a simplification, we choose to linearize the model by assuming $\tilde{k}_{BA}$ is constant. Regardless, one of the major results of this work is that steady state ionic concentrations do not depend strongly on this parameter. By factoring out $[\mathrm{B}]_{\mathrm{cell}}$ from the entire quantity within the parenthesis, we have

$$\phi_{\mathrm{B}} = \tilde{k}_{\mathrm{BA}} [\mathrm{B}]_{\mathrm{cell}} \left([\mathrm{Cl}]_{\mathrm{wall}} - \frac{[\mathrm{Cl}]_{\mathrm{cell}}}{[\mathrm{B}]_{\mathrm{cell}}} [\mathrm{B}]_{\mathrm{wall}} \right). \tag{A.2}$$

Now, we do not explicitly track chloride concentration within our modeling framework. Rather, we track total anion concentration. However, if we define β to be the proportion of total anions at the lumenal wall ($[\mathrm{A}]_{\mathrm{wall}}$) that are, in fact, chloride ($\beta = [\mathrm{Cl}]_{\mathrm{wall}}/[\mathrm{A}]_{\mathrm{wall}}$), then we may rewrite this expression as

$$\phi_{\mathrm{B}} = \tilde{k}_{\mathrm{BA}} \beta [\mathrm{B}]_{\mathrm{cell}} \left([\mathrm{A}]_{\mathrm{wall}} - \frac{[\mathrm{Cl}]_{\mathrm{cell}}}{\beta [\mathrm{B}]_{\mathrm{cell}}} [\mathrm{B}]_{\mathrm{wall}} \right). \tag{A.3}$$

Now, we note that $[\mathrm{A}]_{\mathrm{wall}}$ is our model variable C_{A} evaluated at $x = 0$ and $[\mathrm{B}]_{\mathrm{wall}}$ is our model variable C_{B} evaluated at $x = 0$. We now define our model parameters

$$k_{\mathrm{BA}} = \tilde{k}_{\mathrm{BA}} \beta [\mathrm{B}]_{\mathrm{cell}}, \tag{A.4}$$

and

$$\delta_{\mathrm{BA}} = \frac{[\mathrm{Cl}]_{\mathrm{cell}}}{\beta [\mathrm{B}]_{\mathrm{cell}}} \tag{A.5}$$

to arrive at the given expression for the flux of bicarbonate through the epithelial surface

$$\phi_{\mathrm{B}} = k_{\mathrm{BA}} \left(C_{\mathrm{A}} - \delta_{\mathrm{BA}} C_{\mathrm{B}} \right)\big|_{x=0}. \tag{A.6}$$

Again, we are not able to confidently estimate $\tilde{k}_{\mathrm{BA}}$ (and therefore k_{BA}), so we perform a set of experiments which show the model predictions are not particularly sensitive to this parameter. A rough estimate for intracellular bicarbonate concentration in mammalian cells is $[\mathrm{B}]_{\mathrm{cell}} = 10$ mM [2]. Chloride concentration in mammalian cells varies more than other ionic concentrations (generically), and may range from 5 to 80 mM [2]. However, experiments on frog bladders indicate that epithelial cells may contain chloride concentrations on the high end of this range [20]. For this reason, we choose $[\mathrm{Cl}]_{\mathrm{cell}} = 70$ mM. Obtaining an estimate for β is difficult. Certainly, chloride makes up a large proportion of the anionic content of the stomach lumen (implying β close to one), however, some estimates show that other anions may be present in concentrations which are approximately the same as chloride (implying $\beta \approx 0.5$) [13]. In particular, the relevant quantity in our secretion model is the ratio of chloride to total anion concentration *at the epithelial wall*, but no study that we know of examines how the ionic composition of stomach contents varies spatially across the mucus layer. For this reason, we choose a value of $\beta = 0.7$, which seems well within reasonable estimates. This results in $\delta_{\mathrm{BA}} = 10$.

The same analysis for hydrogen/sodium anti-port exchange gives the expression

$$\phi_{\mathrm{H}} = k_{\mathrm{HI}} \left(C_{\mathrm{I}} - \delta_{\mathrm{HI}} C_{\mathrm{H}}\right)|_{x=0}\,, \tag{A.7}$$

where

$$k_{\mathrm{HI}} = \tilde{k}_{\mathrm{HI}} \alpha [\mathrm{H}]_{\mathrm{cell}}, \tag{A.8}$$

$$\delta_{\mathrm{HI}} = \frac{[\mathrm{Na}]_{\mathrm{cell}}}{\alpha [\mathrm{H}]_{\mathrm{cell}}}, \tag{A.9}$$

and

$$\alpha = \frac{[\mathrm{Na}]_{\mathrm{wall}}}{[\mathrm{I}]_{\mathrm{wall}}} \tag{A.10}$$

is the ratio of sodium to total cation concentration at the wall. To determine the value of δ_{HI}, we use intracellular sodium and hydrogen concentrations of $[\mathrm{Na}]_{\mathrm{cell}} = 10$ mM and $[\mathrm{H}]_{\mathrm{cell}} = 0.2$ µM, which are roughly in line with those reported for mammalian cells in [2]. We choose $\alpha = 0.5$, as potassium is present in the lumen in concentrations roughly equal to sodium [13]. These numbers give $\delta_{\mathrm{HI}} = 10^5$.

Ion Source Magnitude The spatial integral of our source term $S(x)$ physically corresponds to the flux of hydrogen (and corresponding anions) into the system which we impose to mimic Schreiber's hypothesized proton transport process [25]:

$$F = \int S(x)\, dx. \tag{A.11}$$

Physically modeling the process of mucus degradation due to pepsin action is beyond the scope of this work. For this reason we simply choose a spatial profile for $S(x)$. As previously described, the profile is a standard Gaussian function, which is truncated to be zero outside of a small region where the mucus profile (θ_g) transitions from $\theta_g = 0.02$ to approximately zero (for numerical considerations, we ensure that θ_g is always greater than 1×10^{-16}). Therefore we simply scale the magnitude of $S(x)$ to achieve a total flux of hydrogen (F) that is physiologically reasonable. In the human stomach, the secretion of stomach acid may vary dramatically depending on various stimuli (a meal, for example). Secretion rates may range between 1 and 40 mmol/hour [6]. Assuming the human stomach has an interior area of 0.1 m^2, this translates to a flux of secreted hydrogen between 2.78×10^{-7} and 1.11×10^{-5} M cm/sec. As we wish to simulate an "average" stomach, we chose to

perform our experiments with a source $S(x)$ which results in hydrogen flux of $F = 6.11 \times 10^{-6}$ M cm/sec. This is roughly equivalent to a total hydrogen secretion of 22 mmol/hour.

We note here that in the original experiments of [25], the authors report a hydrogen concentration sequestered by mucus of 130 mM. The same paper reports mucus secreted at a rate anywhere between 70 to 570 µm/hour, depending on stimulation. The product of these two quantities is a flux of hydrogen (due to the mechanism proposed by Schreiber, et. al.) anywhere between 3.61×10^{-7} and 2.06×10^{-6} M cm/sec. One criticism that has been leveled at the mechanism proposed by Schreiber, et. al (see [22]) is that these numbers appear to be too low to account for the larger fluxes of hydrogen that may be secreted by either the human [6] or guinea pig stomach [5]. However, the fluxes implied by [25] are not completely incompatible with observed hydrogen fluxes. Furthermore, the series of experiments which determined the sequestration capacity of mucus did not attempt to measure mucus produced during stimulated gastric secretion, nor how it may differ from mucus produced by an unstimulated stomach. Therefore, it is possible that the numbers reported in [25] underestimate the ability of mucus to sequester and transport hydrogen protons.

Table 1: Model Parameters

Parameter	Symbol	Value
Hydrogen Diffusion Coefficient	D_{H}	7×10^{-5} cm^2/sec
Cation Diffusion Coefficient	D_{I}	2.5×10^{-5} cm^2/sec
Bicarbonate Diffusion Coefficient	D_{B}	1.75×10^{-5} cm^2/sec
Anion Diffusion Coefficient	D_{A}	2.5×10^{-5} cm^2/sec
Fluid Volume Flux	$u\theta_s$	1.67×10^{-5} cm/sec
Hydrogen Valence	z_{H}	1
Cation Valence	z_{I}	1
Bicarbonate Valence	z_{B}	-1
Anion Valence	z_{A}	-1
Bicarbonate/Hydrogen Reaction Rate	κ	2.56×10^7 M^{-1} sec^{-1}
Lumenal Hydrogen Concentration	H_L	7.94×10^{-3} M
Lumenal Cation Concentration	I_L	4×10^{-2} M
Lumenal Bicarbonate Concentration	B_L	2.2×10^{-16} M
Lumenal Anion Concentration	A_L	4.79×10^{-2} M
Hydrogen/Cation Exchange Bias	δ_{HI}	1×10^5
Bicarbonate/Anion Exchange Bias	δ_{BA}	10
Hydrogen/Cation Exchange Rate	k_{HI}	1×10^{-6} – 0.1 cm/sec
Bicarbonate/Anion Exchange Rate	k_{BA}	1×10^{-6} – 0.1 cm/sec

B Numerical Scheme

Here we outline the discretization that is utilized to simulate the system of eqs. (1) and (2). In many ways, our technique is a standard second-order finite volume discretization in space, combined with a first-order implicit-explicit (IMEX) time integration scheme [3]. However, we were forced to make several modifications to the standard numerical techniques in order to account for various nonlinear terms. We begin by discretizing space using a so-called "staggered grid". Two collections of spacial points are defined, and various quantities more naturally "live" at each. The first collection of

points we refer to as "cell edges," and they are defined by

$$x_j = j\,\Delta x \quad j = 0, 1, \ldots N \tag{B.1}$$

where $\Delta x = L/N$ is the spatial resolution of the grid. The second collection of points are referred to as "cell centers" and are defined by

$$x_j = j\,\Delta x \quad j = \frac{-1}{2}, \frac{1}{2}, \frac{3}{2} \ldots N + \frac{1}{2}. \tag{B.2}$$

There are in total $N+1$ cell edges and $N+2$ cell centers, but not all correspond to spatial locations within our domain. The cell edges x_0 and x_N, as well as the cell centers $x_{1/2}$ and $x_{N+1/2}$ lie either at, or outside the boundary of the computational domain. These are often called "ghost points" and quantities located at them are a numerical convenience used to help enforce boundary conditions, but may not necessarily correspond to a physical quantity. All other points lie within the domain and will be referred to as interior cell centers and interior cell edges. A schematic of the spatial discretization is shown in fig. B.1. Finally, we have a single temporal discretization

$$t_n = n\,\Delta t, \quad n = 0, 1, \ldots \tag{B.3}$$

We approximate ionic concentrations at cell centers. Where necessary, we use a second subscript j to denote the spatial location where an approximation takes place, while a superscript n denotes the temporal location.

$$C^n_{i,\,j} \approx C_i(x_j, t_n), \quad i = \mathrm{H}, \mathrm{B}, \mathrm{A}, \mathrm{I}. \tag{B.4}$$

Finally, we introduce the quantity Φ to approximate the electric potential gradient. This quantity "lives" at cell edges ($j = 0, 1, \ldots N$).

$$\Phi^n_j \approx \nabla\Psi(x_j, t_n). \tag{B.5}$$

To approximate the Nernst-Planck type equation at interior cell centers, we use standard finite-difference and finite volume discretizations for all linear terms. The advective flux is treated with a standard explicit upwinding scheme, while the diffusive flux is treated with a standard implicit second order, variable coefficient, finite difference scheme [18]. However, the electric flux term and buffering reaction term both involve nonlinear products of two model variables. Therefore, we treat these terms semi-implicitly in time. To do so requires extrapolating "forward" in time. We use first order extrapolation whenever possible, and zeroth order whenever we must (i.e. at the very first time step). Doing so allows us to define the quantities

$$\tilde{C}^{n+1}_{i,\,j} = \begin{cases} 2C^n_{i,\,j} - C^{n-1}_{i,\,j}, & n \geq 1 \\ C^n_{i,\,j}, & n = 0 \end{cases}, \quad i = \mathrm{H}, \mathrm{B}, \mathrm{A}, \mathrm{I}. \tag{B.6}$$

Finally, we utilize the same "second subscript" notation to denote the solvent volume fraction $\theta_s(x)$ at various spatial locations, though we note here no approximation is necessary as we can simply evaluate the given function.

We are now able to discretize eq. (1) for each of the four ionic species, at each interior cell center

$(j = 1/2, 3/2, \ldots N - 1/2)$:

$$\frac{C_{H,\,j}^{n+1} - C_{H,\,j}^{n}}{\Delta t} + \frac{u\left(C_{H,\,j}^{n} - C_{H,\,j-1}^{n}\right)}{\Delta x} = \frac{D_{\mathrm{H}}}{\theta_{s,\,j}\Delta x^2}\left(\left(\theta_{s,\,j-1/2}\right)C_{H,\,j-1}^{n+1} - \left(\theta_{s,\,j-1/2} + \theta_{s,\,j+1/2}\right)C_{H,\,j}^{n+1} + \left(\theta_{s,\,j+1/2}\right)C_{H,\,j+1}^{n+1}\right) + \frac{D_{\mathrm{H}} z_{\mathrm{H}}}{\theta_{s,\,j}\Delta x}\left(\theta_{s,\,j+1/2}\left(\frac{\tilde{C}_{H,\,j+1}^{n+1} + \tilde{C}_{H,\,j}^{n+1}}{2}\right)\Phi_{j+1/2}^{n+1} - \theta_{s,\,j-1/2}\left(\frac{\tilde{C}_{H,\,j}^{n+1} + \tilde{C}_{H,\,j-1}^{n+1}}{2}\right)\Phi_{j-1/2}^{n+1}\right) + S(x_j) - \kappa\left(C_{H,\,j}^{n+1}\tilde{C}_{B,\,j}^{n+1}\right), \quad \text{(B.7)}$$

$$\frac{C_{B,\,j}^{n+1} - C_{B,\,j}^{n}}{\Delta t} + \frac{u\left(C_{B,\,j}^{n} - C_{B,\,j-1}^{n}\right)}{\Delta x} = \frac{D_{\mathrm{H}}}{\theta_{s,\,j}\Delta x^2}\left(\left(\theta_{s,\,j-1/2}\right)C_{B,\,j-1}^{n+1} - \left(\theta_{s,\,j-1/2} + \theta_{s,\,j+1/2}\right)C_{B,\,j}^{n+1} + \left(\theta_{s,\,j+1/2}\right)C_{B,\,j+1}^{n+1}\right) + \frac{D_{\mathrm{H}} z_{\mathrm{H}}}{\theta_{s,\,j}\Delta x}\left(\theta_{s,\,j+1/2}\left(\frac{\tilde{C}_{B,\,j+1}^{n+1} + \tilde{C}_{B,\,j}^{n+1}}{2}\right)\Phi_{j+1/2}^{n+1} - \theta_{s,\,j-1/2}\left(\frac{\tilde{C}_{B,\,j}^{n+1} + \tilde{C}_{B,\,j-1}^{n+1}}{2}\right)\Phi_{j-1/2}^{n+1}\right) - \kappa\left(C_{B,\,j}^{n+1}\tilde{C}_{H,\,j}^{n+1}\right), \quad \text{(B.8)}$$

$$\frac{C_{A,\,j}^{n+1} - C_{A,\,j}^{n}}{\Delta t} + \frac{u\left(C_{A,\,j}^{n} - C_{A,\,j-1}^{n}\right)}{\Delta x} = \frac{D_{\mathrm{H}}}{\theta_{s,\,j}\Delta x^2}\left(\left(\theta_{s,\,j-1/2}\right)C_{A,\,j-1}^{n+1} - \left(\theta_{s,\,j-1/2} + \theta_{s,\,j+1/2}\right)C_{A,\,j}^{n+1} + \left(\theta_{s,\,j+1/2}\right)C_{A,\,j+1}^{n+1}\right) + \frac{D_{\mathrm{H}} z_{\mathrm{H}}}{\theta_{s,\,j}\Delta x}\left(\theta_{s,\,j+1/2}\left(\frac{\tilde{C}_{A,\,j+1}^{n+1} + \tilde{C}_{A,\,j}^{n+1}}{2}\right)\Phi_{j+1/2}^{n+1} - \theta_{s,\,j-1/2}\left(\frac{\tilde{C}_{A,\,j}^{n+1} + \tilde{C}_{A,\,j-1}^{n+1}}{2}\right)\Phi_{j-1/2}^{n+1}\right) + S(x_j), \quad \text{(B.9)}$$

$$\frac{C_{I,\,j}^{n+1} - C_{I,\,j}^{n}}{\Delta t} + \frac{u\left(C_{I,\,j}^{n} - C_{I,\,j-1}^{n}\right)}{\Delta x} = \frac{D_{\mathrm{H}}}{\theta_{s,\,j}\Delta x^2}\left(\left(\theta_{s,\,j-1/2}\right)C_{I,\,j-1}^{n+1} - \left(\theta_{s,\,j-1/2} + \theta_{s,\,j+1/2}\right)C_{I,\,j}^{n+1} + \left(\theta_{s,\,j+1/2}\right)C_{I,\,j+1}^{n+1}\right) + \frac{D_{\mathrm{H}} z_{\mathrm{H}}}{\theta_{s,\,j}\Delta x}\left(\theta_{s,\,j+1/2}\left(\frac{\tilde{C}_{I,\,j+1}^{n+1} + \tilde{C}_{I,\,j}^{n+1}}{2}\right)\Phi_{j+1/2}^{n+1} - \theta_{s,\,j-1/2}\left(\frac{\tilde{C}_{I,\,j}^{n+1} + \tilde{C}_{I,\,j-1}^{n+1}}{2}\right)\Phi_{j-1/2}^{n+1}\right). \quad \text{(B.10)}$$

We also discretize the boundary conditions for each species implicitly in time except (again) for the nonlinear term which represents the electric flux. To approximate ionic species *at* a boundary, we utilize linear interpolation (in space) using ghost points and the first interior cell center. At the

left boundary of our domain (where $j = 0$) we have the following equations:

$$k_{\mathrm{HI}}\left(\frac{C^{n+1}_{I,\,-1/2}+C^{n+1}_{I,\,1/2}}{2}-\delta_{HI}\frac{C^{n+1}_{H,\,-1/2}+C^{n+1}_{H,\,1/2}}{2}\right)= \\ -\frac{D_{\mathrm{H}}}{\Delta x}\left(C^{n+1}_{H,\,1/2}-C^{n+1}_{H,\,-1/2}\right)+uC^{n+1}_{H,\,-1/2}-D_{\mathrm{H}}z_{\mathrm{H}}\left(\frac{\tilde{C}^{n+1}_{H,\,-1/2}+\tilde{C}^{n+1}_{H,\,1/2}}{2}\right)\Phi_0^{n+1}, \quad \text{(B.11)}$$

$$-k_{\mathrm{HI}}\left(\frac{C^{n+1}_{I,\,-1/2}+C^{n+1}_{I,\,1/2}}{2}-\delta_{HI}\frac{C^{n+1}_{H,\,-1/2}+C^{n+1}_{H,\,1/2}}{2}\right)= \\ -\frac{D_{\mathrm{I}}}{\Delta x}\left(C^{n+1}_{I,\,1/2}-C^{n+1}_{I,\,-1/2}\right)+uC^{n+1}_{I,\,-1/2}-D_{\mathrm{I}}z_{\mathrm{I}}\left(\frac{\tilde{C}^{n+1}_{I,\,-1/2}+\tilde{C}^{n+1}_{I,\,1/2}}{2}\right)\Phi_0^{n+1}, \quad \text{(B.12)}$$

$$k_{\mathrm{BA}}\left(\frac{C^{n+1}_{A,\,-1/2}+C^{n+1}_{A,\,1/2}}{2}-\delta_{BA}\frac{C^{n+1}_{B,\,-1/2}+C^{n+1}_{B,\,1/2}}{2}\right)= \\ -\frac{D_{\mathrm{B}}}{\Delta x}\left(C^{n+1}_{B,\,1/2}-C^{n+1}_{B,\,-1/2}\right)+uC^{n+1}_{B,\,-1/2}-D_{\mathrm{B}}z_{\mathrm{B}}\left(\frac{\tilde{C}^{n+1}_{B,\,-1/2}+\tilde{C}^{n+1}_{B,\,1/2}}{2}\right)\Phi_0^{n+1}, \quad \text{(B.13)}$$

$$-k_{\mathrm{BA}}\left(\frac{C^{n+1}_{A,\,-1/2}+C^{n+1}_{A,\,1/2}}{2}-\delta_{BA}\frac{C^{n+1}_{B,\,-1/2}+C^{n+1}_{B,\,1/2}}{2}\right)= \\ -\frac{D_{\mathrm{A}}}{\Delta x}\left(C^{n+1}_{A,\,1/2}-C^{n+1}_{A,\,-1/2}\right)+uC^{n+1}_{A,\,-1/2}-D_{\mathrm{A}}z_{\mathrm{A}}\left(\frac{\tilde{C}^{n+1}_{A,\,-1/2}+\tilde{C}^{n+1}_{A,\,1/2}}{2}\right)\Phi_0^{n+1}. \quad \text{(B.14)}$$

The boundary conditions at the right are significantly simpler:

$$\frac{C^{n+1}_{H,\,N-1/2}+C^{n+1}_{H,\,N+1/2}}{2}=H_L, \quad \text{(B.15)}$$

$$\frac{C^{n+1}_{B,\,N-1/2}+C^{n+1}_{B,\,N+1/2}}{2}=B_L, \quad \text{(B.16)}$$

$$\frac{C^{n+1}_{A,\,N-1/2}+C^{n+1}_{A,\,N+1/2}}{2}=A_L, \quad \text{(B.17)}$$

$$\frac{C^{n+1}_{I,\,N-1/2}+C^{n+1}_{I,\,N+1/2}}{2}=I_L, \quad \text{(B.18)}$$

Finally, we have a set of discrete equations which enforce the electro-neutrality constraint at the the interior cell centers ($j = 1/2, 3/2, \ldots N-1/2$) *as well as the ghost point corresponding to* $j = -1/2$.

$$z_H C^{n+1}_{H,\,j}+z_B C^{n+1}_{B,\,j}+z_A C^{n+1}_{A,\,j}+z_I C^{n+1}_{I,\,j}=0, \quad j=-1/2,1/2,\ldots N-1/2. \quad \text{(B.19)}$$

We enforce the electro-neutrality constraint at the left most ghost point even though the concentrations at this point do not represent physical quantities. This is done to ensure that (up to linear

approximation), the electro-neutrality constraint is satisfied up to and including the left boundary. We do not need a similar equation at the right ghost cell center because eqs. (B.15) to (B.18) together with choosing H_L, B_L, A_L and I_L satisfying electro-neturality imply this condition is already met.

Now, at a given time t_n, the concentrations $C^n_{i,j}$ are known for $j = -1/2, 1/2, \ldots N + 1/2$ and $i = \mathrm{H}, \mathrm{I}, \mathrm{A}, \mathrm{B}$. So is the approximate electric potential gradient Φ^n_j for $j = 0, 1, \ldots N$. We then extrapolate forward in time to find $\tilde{C}^{n+1}_{i,j}$, which is necessary for our semi-implicit treatment of nonlinear terms. Once these quantities are known, eqs. (B.7) to (B.19) represent a system of linear equations which may be solved for concentrations and the potential gradient (simultaneously) at the next time step ($C^{n+1}_{i,j}$ and Φ^{n+1}_j). The system is integrated forward in time in this manner. The explicit treatment of the advective flux requires that we satisfy a numerical CFL condition

$$\Delta t < \frac{\Delta x}{u}.$$

However, our semi-implicit treatment of the nonlinear buffering reaction drastically relaxes the time-step restrictions which would normally be associated with the extremely stiff buffering reaction. Similarly, the fact that we treat the nonlinear electric flux semi-implicitly and solve for the electric potential gradient and concentrations *simultaneously* alleviates the stiffness that would normally be associated with time-splitting the system (updating concentrations and potential gradient sequentially).

We refined in space and time (decreased Δx and Δt by a factor of 2 each) until refining the simulation resulted in less than 2% change in steady state concentrations. In our experience, this was true with $\Delta x = 1 \times 10^{-3}$ cm (which corresponds to $N = 200$ interior cell centers) and $\Delta t = 5 \times 10^{-4}$ sec. However, for extra graphical clarity we ran nearly all simulations at twice this resolution, with $\Delta x = 5 \times 10^{-4}$ cm (which corresponds to $N = 400$ interior cell centers) and $\Delta t = 2.5 \times 10^{-4}$ sec. The only exceptions to this were the simulations used to generate the first panel of fig. 3. The shear number of data points necessary to produce this graph rendered this simulation extremely time intensive. Therefore this graph was generated using simulations with $\Delta x = 1 \times 10^{-3}$ cm and $\Delta t = 5 \times 10^{-4}$ sec. The source code used to perform these simulations is publicly available at `https://github.com/OwenLewis/Mucus_pH_diffus`.

References

[1] Allen, A., and Flemström, G. Gastroduodenal Mucus Bicarbonate Barrier: Protection Against Acid and Pepsin. *American Journal of Physiology - Cell Physiology 288*, 1 (Jan. 2005), C1–19.

[2] Andersen, O. S. Cellular Electrolyte Metabolism. In *Encyclopedia of Metalloproteins*. Springer New York, New York, NY, 2013, pp. 580–587.

[3] Ascher, U. M., Ruuth, S. J., and Wetton, B. T. R. Implicit-explicit methods for time-dependent partial differential equations. *SIAM Journal on Numerical Analysis 32*, 3 (1995), 797–823.

[4] Bahari, H. M., Ross, I. N., and Turnberg, L. A. Demonstration of a pH Gradient Across the Mucus Layer on the Surface of Human Gastric Mucosa in Vitro. *Gut 23*, 6 (June 1982), 513–516.

[5] Batzri, S., Harmon, J. W., Dubois, A., Moskowitz, D., Weichbrod, R., and Rich, N. M. A New in Vivo Method for Repeatedly Studying Gastric Acid Secretion and Other Secretory Parameters in Awake Guinea Pig. *The Journal of Surgical Research 43*, 5 (Nov. 1987), 398–406.

[6] Berne, R. M., and Levy, M. N. *Physiology*, third ed. Mosby, St. Louis, 1993.

[7] Chu, S., Tanaka, S., Kaunitz, J. D., and Montrose, M. H. Dynamic Regulation of Gastric Surface pH by Luminal pH. *Journal of Clinical Investigation 103*, 5 (Mar. 1999), 605–612.

[8] Coskun, T., Chu, S., and Montrose, M. H. Intragastric pH Regulates Conversion From Net Acid to Net Alkaline Secretion by the Rat Stomach. *American Journal of Physiology - Gastrointestinal and Liver Physiology 281*, 4 (Oct. 2001), G870–7.

[9] Cussler, E. L. *Diffusion: Mass Transfer in Fluid Systems*, 3 ed. Cambridge University Press, 2009.

[10] Engel, E., Guth, P. H., Nishizaki, Y., and Kaunitz, J. D. Barrier Function of the Gastric Mucus Gel. *American Journal of Physiology 269*, 6 Pt 1 (Dec. 1995), G994–9.

[11] Engel, E., Peskoff, A., Kauffman, G. L., and Grossman, M. I. Analysis of Hydrogen Ion Concentration in the Gastric Gel Mucus Layer. *American Journal of Physiology 247*, 4 Pt 1 (Oct. 1984), G321–38.

[12] Flemström, G., and Isenberg, J. I. Gastroduodenal Mucosal Alkaline Secretion and Mucosal Protection. *News in Physiological Sciences 16* (Feb. 2001), 23–28.

[13] Fordtran, J. S., and Locklear, T. W. Ionic Constituents and Osmolality of Gastric and Small-Intestinal Fluids After Eating. *The American Journal of Digestive Diseases 11*, 7 (July 1966), 503–521.

[14] Haynes, W. M., Lide, D. R., and Bruno, T. J., Eds. *CRC Handbook of Chemistry and Physics, 95th Edition*, 95 ed. CRC Press, 2014.

[15] Holm, L., and Flemström, G. Microscopy of Acid Transport at the Gastric Surface in Vivo. *Journal of Internal Medicine. Supplement 732* (1990), 91–95.

[16] Johansson, M., Synnerstad, I., and Holm, L. Acid Transport Through Channels in the Mucous Layer of Rat Stomach. *Gastroenterology 119*, 5 (Nov. 2000), 1297–1304.

[17] Keener, J., and Sneyd, J. *Mathematical Physiology. Vol. I: Cellular Physiology*, second ed., vol. 8/ of *Interdisciplinary Applied Mathematics*. Springer, New York, New York, NY, 2009.

[18] Leveque, R. J. *Finite Difference Methods for Ordinary and Partial Differential Equations*. Steady-State and Time-Dependent Problems. Society for Industrial and Applied Mathematics, 2007.

[19] Li, L., Lieleg, O., Jang, S., Ribbeck, K., and Han, J. A Microfluidic in Vitro System for the Quantitative Study of the Stomach Mucus Barrier Function. *Lab On a Chip 12*, 20 (Oct. 2012), 4071–4079.

[20] Macknight, A. D., Dibona, D. R., Leaf, A., and Civan, M. M. Measurement of the Composition of Epithelial Cells From the Toad Urinary Bladder. *The Journal of Membrane Biology 6*, 2 (June 1971), 108–126.

[21] Odes, H. S., Hogan, D. L., Steinbach, J. H., Ballesteros, M. A., Koss, M. A., and Isenberg, J. I. Measurement of gastric bicarbonate secretion in the human stomach: different methods produce discordant results. *Scandinavian Journal of Gastroenterology 27*, 10 (Oct. 1992), 829–836.

[22] Phillipson, M. M. Acid Transport Through Gastric Mucus. *Upsala Journal of Medical Sciences 109*, 1 (Jan. 2004), 1–24.

[23] Riddell, M. J., Strong, J. A., and Cameron, D. The Electrolyte Concentration of Human Gastric Secretion. *Quarterly Journal of Experimental Physiology and Cognate Medical Sciences 45*, 1 (1960), 1–11.

[24] Schreiber, S., Nguyen, T. H., Stüben, M., and Scheid, P. Demonstration of a pH Gradient in the Gastric Gland of the Acid-Secreting Guinea Pig Mucosa. *American Journal of Physiology - Gastrointestinal and Liver Physiology 279*, 3 (Sept. 2000), G597–G604.

[25] Schreiber, S. S., and Scheid, P. P. Gastric Mucus of the Guinea Pig: Proton Carrier and Diffusion Barrier. *American Journal of Physiology 272*, 1 Pt 1 (Jan. 1997), G63–G70.

[26] Schubert, M. L. Gastric Secretion. *Current Opinion in Gastroenterology 20*, 6 (Nov. 2004), 519–525.

[27] Sircar, S., Keener, J. P., and Fogelson, A. L. The Effect of Divalent vs. Monovalent Ions on the Swelling of Mucin-Like Polyelectrolyte Gels: Governing Equations and Equilibrium Analysis. *The Journal of Chemical Physics 138*, 1 (Jan. 2013), 014901–014901.

[28] Tinoco, I., Sauer, K., Wang, J. C., and Puglisi, J. D. *Physical Chemistry*, 4th ed. Principles and Applications in Biological Sciences. Prentice Hall, Upper Saddle River, New Jersey, 2002.

[29] Williams, S. E., and Turnberg, L. A. Retardation of Acid Diffusion by Pig Gastric Mucosa: a Potential Role in Mucosal Protection. *Gastroenterology 79*, 2 (Aug. 1980), 299–304.

[30] Williams, S. E., and Turnberg, L. A. Demonstration of a pH Gradient Across Mucus Adherent to Rabbit Gastric Mucosa: Evidence for a 'Mucus-Bicarbonate' Barrier. *Gut 22*, 2 (Feb. 1981), 94–96.

[31] Zeebe, R. E. On the Molecular Diffusion Coefficients of Dissolved CO,HCO3-, and CO32- and Their Dependence on Isotopic Mass. *Geochimica et Cosmochimica Acta 75*, 9 (May 2011), 2483–2498.

Figure 1: Illustration of gel volume fraction (θ_g) and Hydrogen/Anion source profiles. Recall that $\theta_s = 1 - \theta_g$.

Figure 2: Left panel shows the base case steady state ion concentrations in the domain (produced with $k_{\mathrm{HI}} = k_{\mathrm{BA}} = 2 \times 10^{-4}$ cm/sec). Right panel shows the flux of hydrogen ions at steady state, as well as how the total flux is partitioned into diffusive, advective, and electric fluxes. In each case, the inset shows a zoomed view of the same data near the wall. Grey shaded regions indicate the mucus layer where $\theta_g \geq 0.01$.

Figure 3: The first panel shows wall pH as a function of hydrogen/cation and bicarbonate/anion exchange rates (k_{HI} and k_{BA} respectively). The solid line indicates parameter values that result in a wall pH of 6. The two dash-dot lines indicate $k_{\mathrm{HI}} = 2 \times 10^{-6}$ and 2×10^{-4} cm/sec, which are the parameter values used to generate the data in the second panel. The dashed line indicates the largest value of k_{BA} which results in a monotonic profile of hydrogen ions. The black dot indicates the parameter values that we refer to as "base case." The second panel shows wall pH as a function of k_{BA} for the two values of k_{HI} indicated in the left panel.

Figure 4: Left panel shows the base case steady state ion concentration in the stomach (produced with $k_{\mathrm{HI}} = 1 \times 10^{-1}$ cm/sec and $k_{\mathrm{BA}} = 5 \times 10^{-4}$ cm/sec). Right panel shows the corresponding fluxes of hydrogen ions at steady state. Grey shaded regions indicate the mucus layer where $\theta_g \geq 0.01$.

Figure 5: First panel shows pH at the stomach wall as a function of lumen pH. Second panel shows the flux due to various sources of ions as a function of lumenal pH. The flux due to hydrogen source is calculated as $\int S(x)\, dx$. The fluxes through the wall are a result of the ion exchange relationship. All data were generated using the "base case" for k_{HI} and k_{BA}.

Figure 6: pH at stomach wall as a function of bicarbonate exchanger rate for three different lumen salt concentrations. Left panel shows the case when hydrogen/cation exchange proceeds normally ($k_{\mathrm{HI}} = 2 \times 10^{-4}$ cm/sec) and right panel shows the case when hydrogen/cation exchange is completely inhibited ($k_{\mathrm{HI}} = 0$).

Figure B.1: A schematic representation of our computational grid for $N = 5$. Dashed vertical black lines indicate the boundaries of the computational domain. Circles indicate cell centers, while diamonds indicate cell edges. Interior points are drawn with solid lines while ghost points are drawn with dash-dot lines.

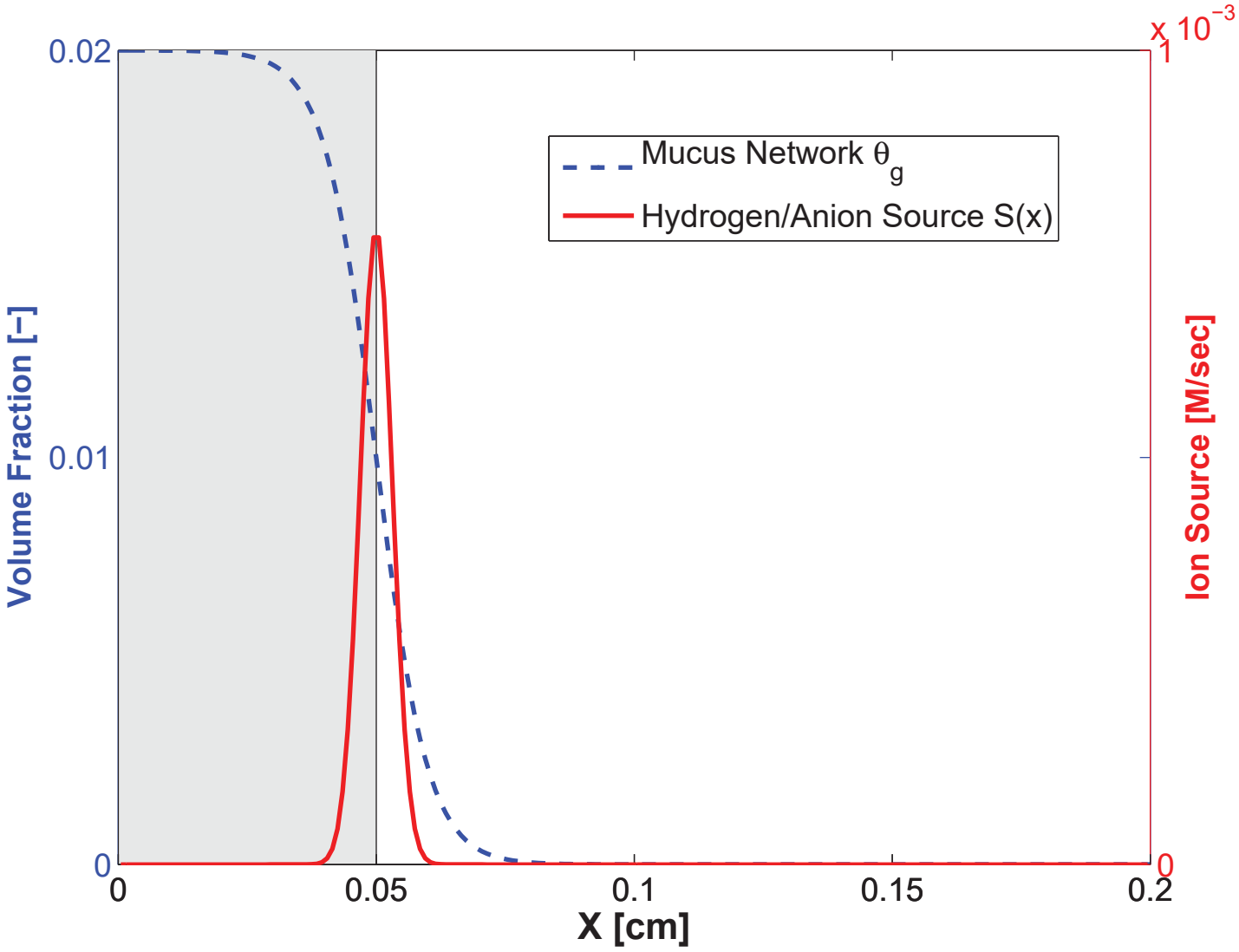
0.02
0.01
0
0
0.05
0.1
0.15
0.2
X [cm]
Volume Fraction [–]
Ion Source [M/sec]
x 10^-3
1
0
Mucus Network θg
Hydrogen/Anion Source S(x)

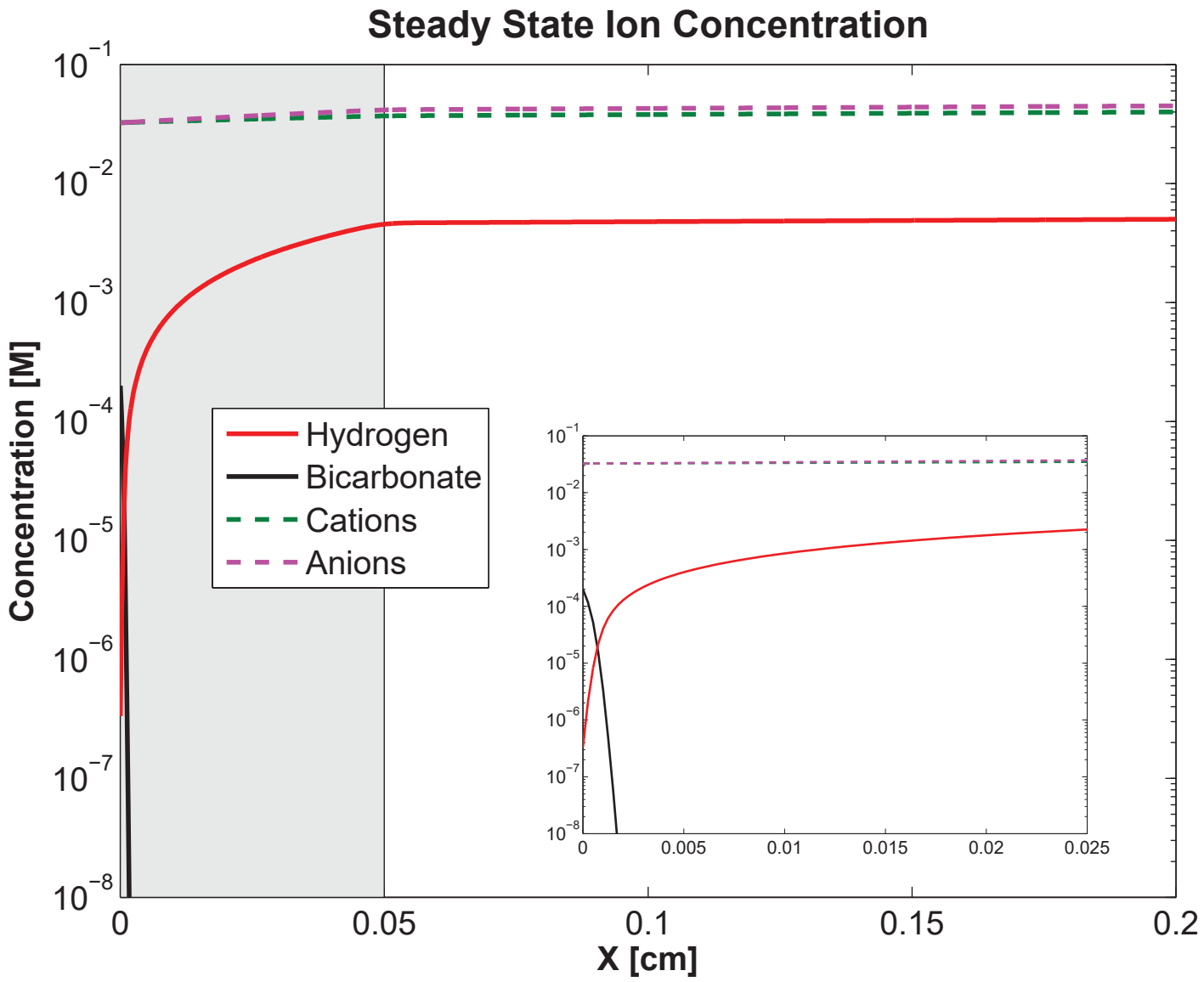
Steady State Ion Concentration
Concentration [M]
X [cm]
Hydrogen
Bicarbonate
Cations
Anions
10^-1
10^-2
10^-3
10^-4
10^-5
10^-6
10^-7
10^-8
0
0.05
0.1
0.15
0.2
0.005
0.01
0.015
0.02
0.025

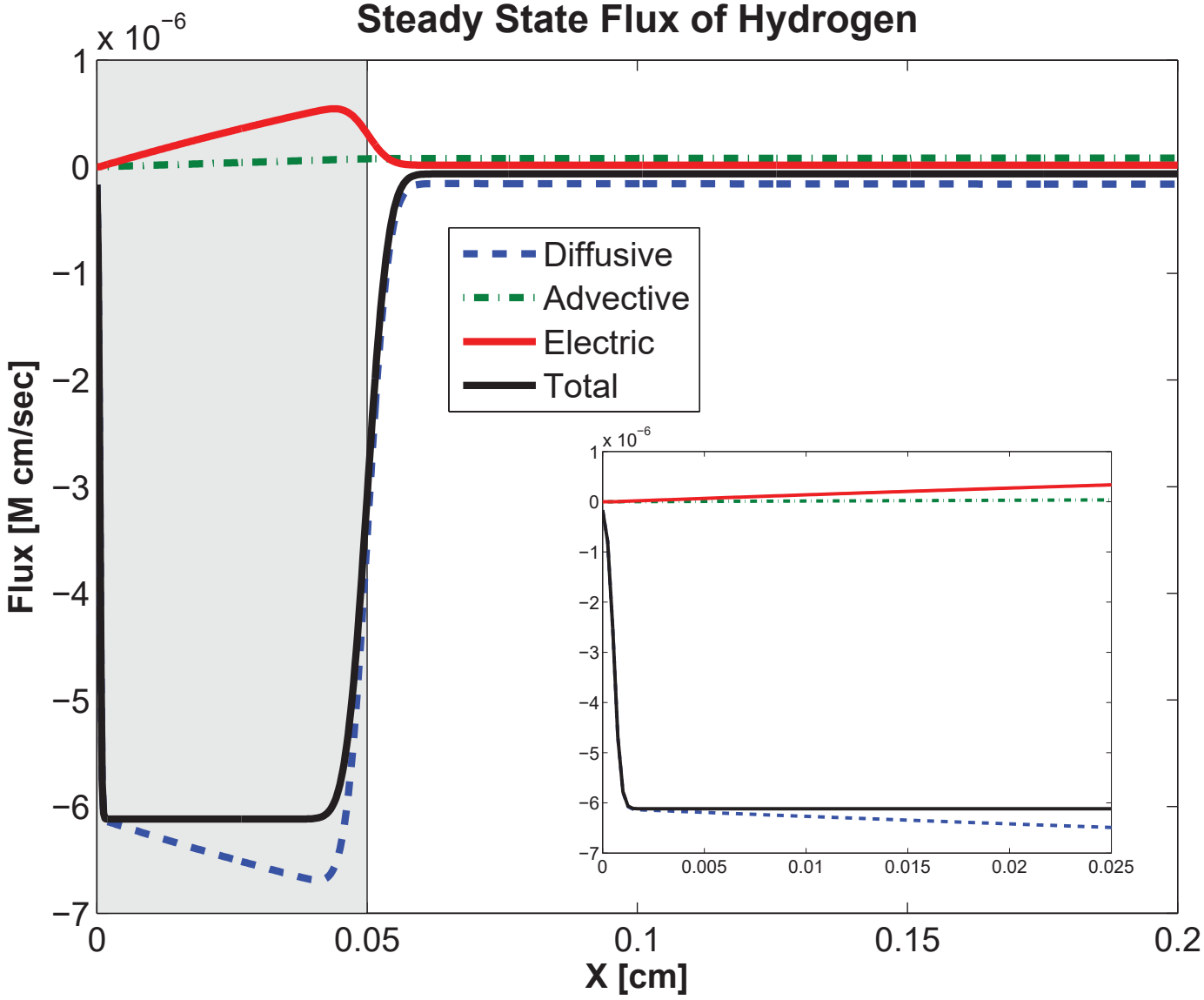
Steady State Flux of Hydrogen
x 10^−6
1
0
−1
−2
−3
−4
−5
−6
−7
Flux [M cm/sec]
0
0.05
0.1
0.15
0.2
X [cm]
Diffusive
Advective
Electric
Total
x 10^−6
1
0
−1
−2
−3
−4
−5
−6
−7
0
0.005
0.01
0.015
0.02
0.025

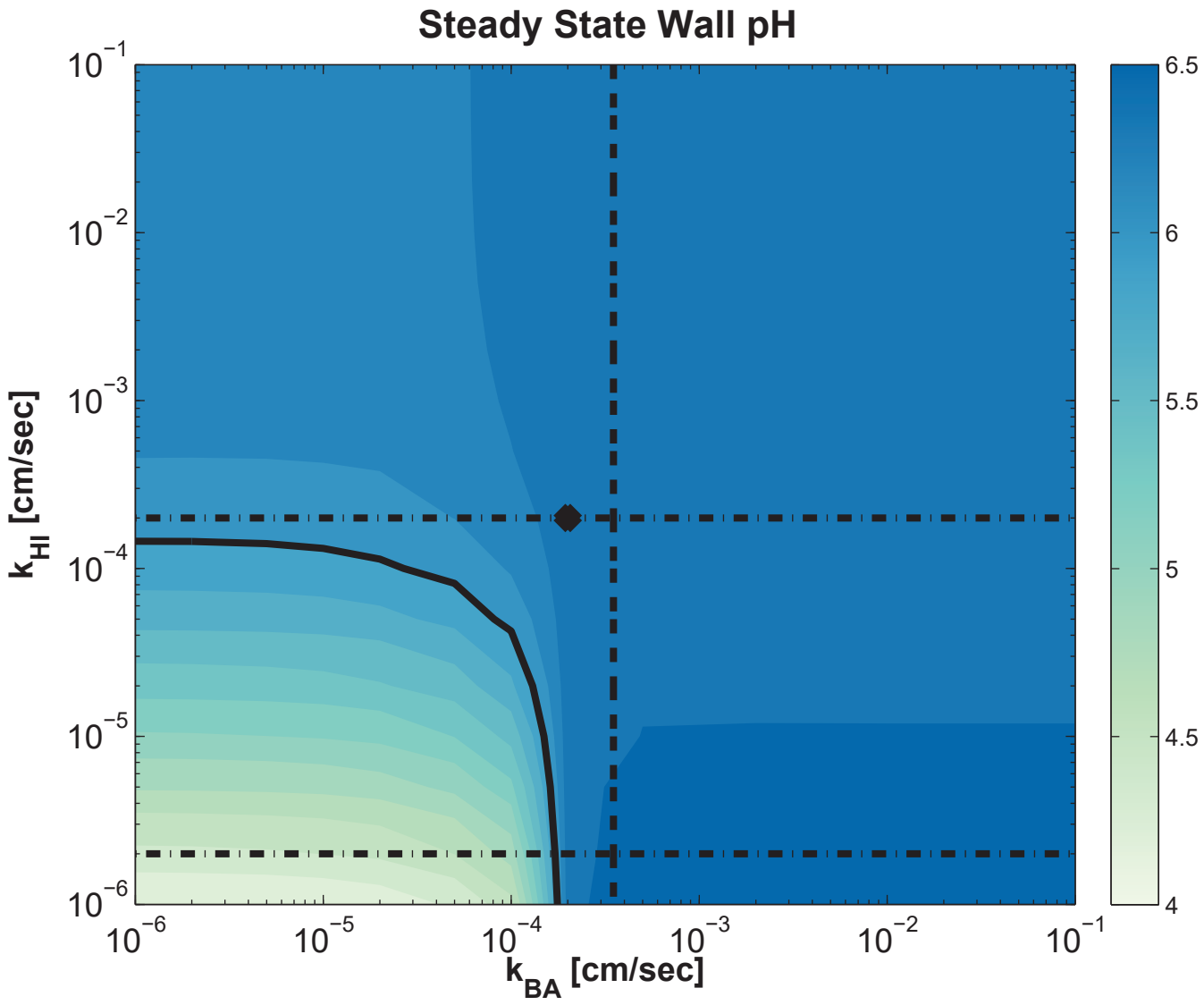
Steady State Wall pH
10^{-1}
10^{-2}
10^{-3}
10^{-4}
10^{-5}
10^{-6}
k_{HI} [cm/sec]
10^{-6}
10^{-5}
10^{-4}
10^{-3}
10^{-2}
10^{-1}
k_{BA} [cm/sec]
6.5
6
5.5
5
4.5
4

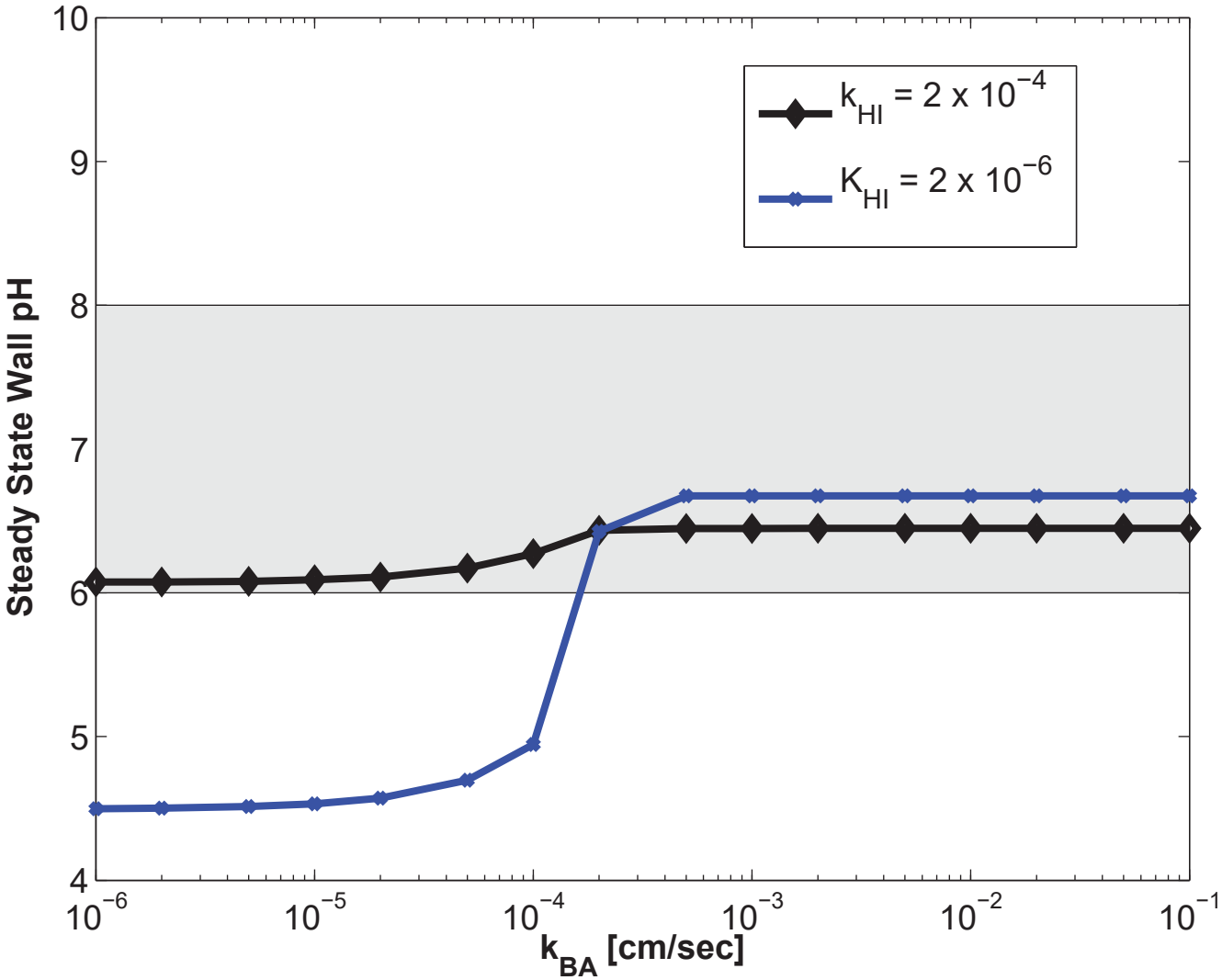
10
9
8
7
6
5
4
Steady State Wall pH
k_{HI} = 2 x 10^{-4}
K_{HI} = 2 x 10^{-6}
10^{-6}
10^{-5}
10^{-4}
10^{-3}
10^{-2}
10^{-1}
k_{BA} [cm/sec]

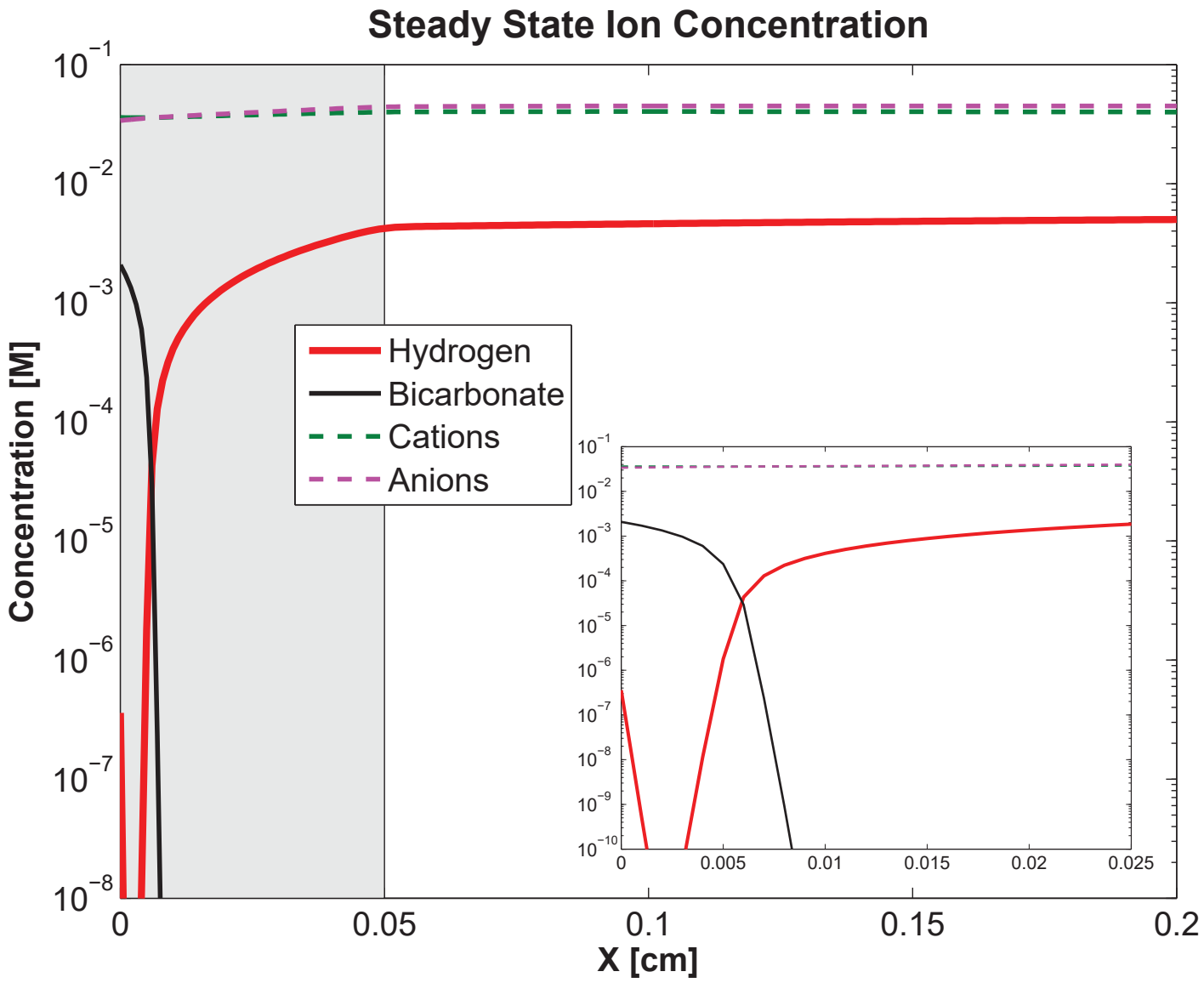
Steady State Ion Concentration
Concentration [M]
X [cm]
Hydrogen
Bicarbonate
Cations
Anions
10^-1
10^-2
10^-3
10^-4
10^-5
10^-6
10^-7
10^-8
0
0.05
0.1
0.15
0.2
10^-1
10^-2
10^-3
10^-4
10^-5
10^-6
10^-7
10^-8
10^-9
10^-10
0
0.005
0.01
0.015
0.02
0.025

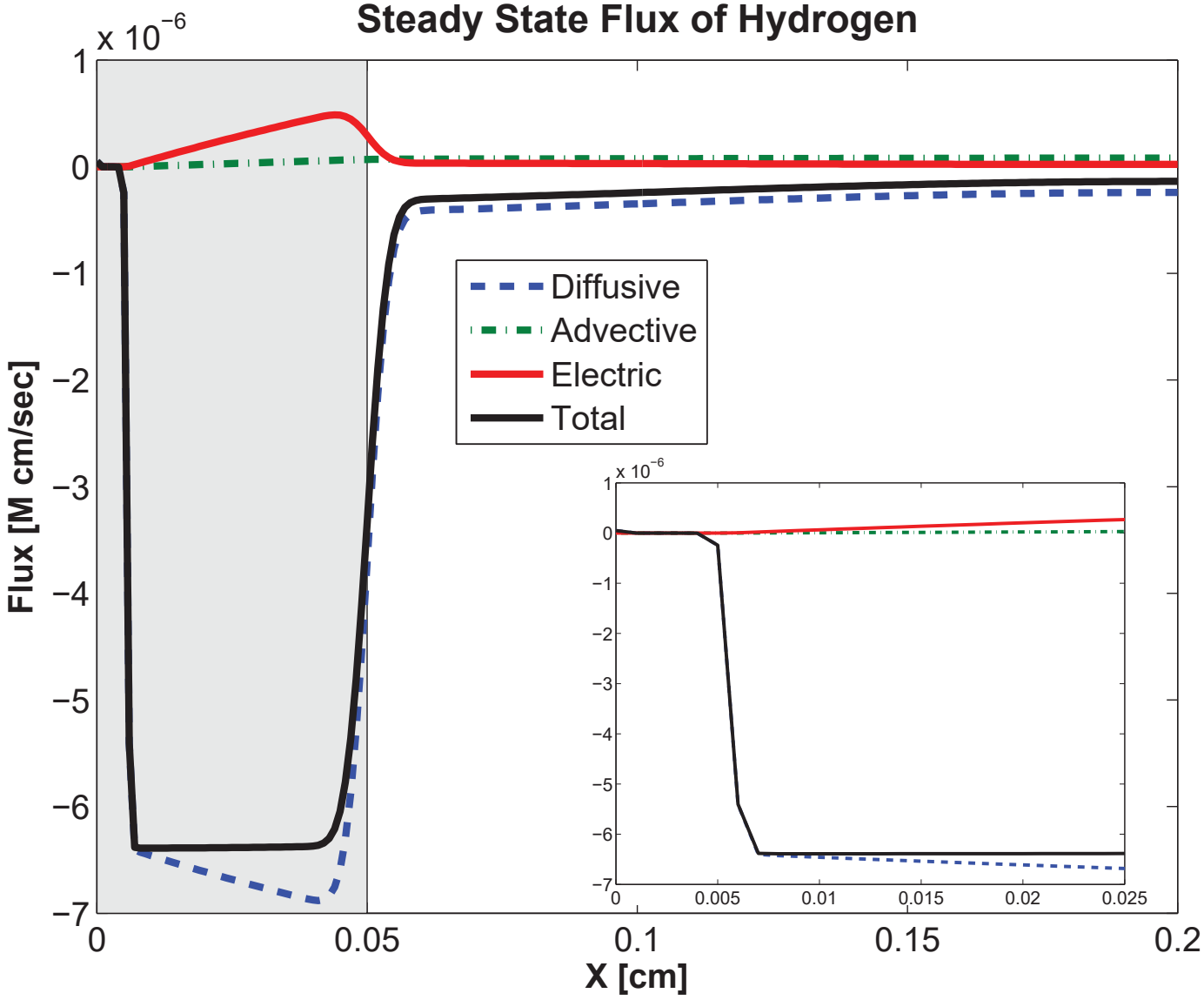
Steady State Flux of Hydrogen
x 10^−6
Flux [M cm/sec]
X [cm]
Diffusive
Advective
Electric
Total
1
0
−1
−2
−3
−4
−5
−6
−7
0
0.05
0.1
0.15
0.2
0.005
0.01
0.015
0.02
0.025

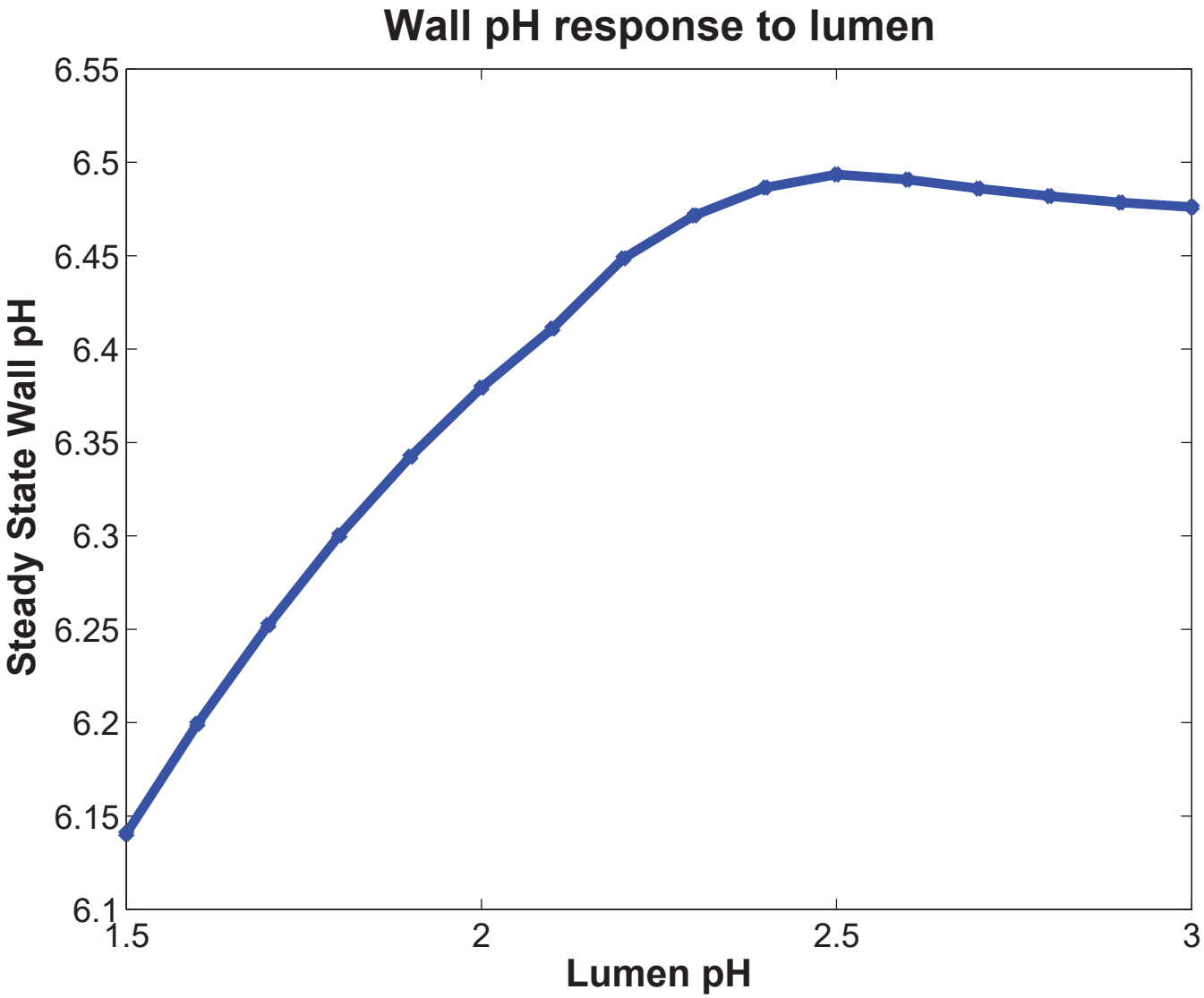
Wall pH response to lumen
Steady State Wall pH
6.55
6.5
6.45
6.4
6.35
6.3
6.25
6.2
6.15
6.1
1.5
2
2.5
3
Lumen pH

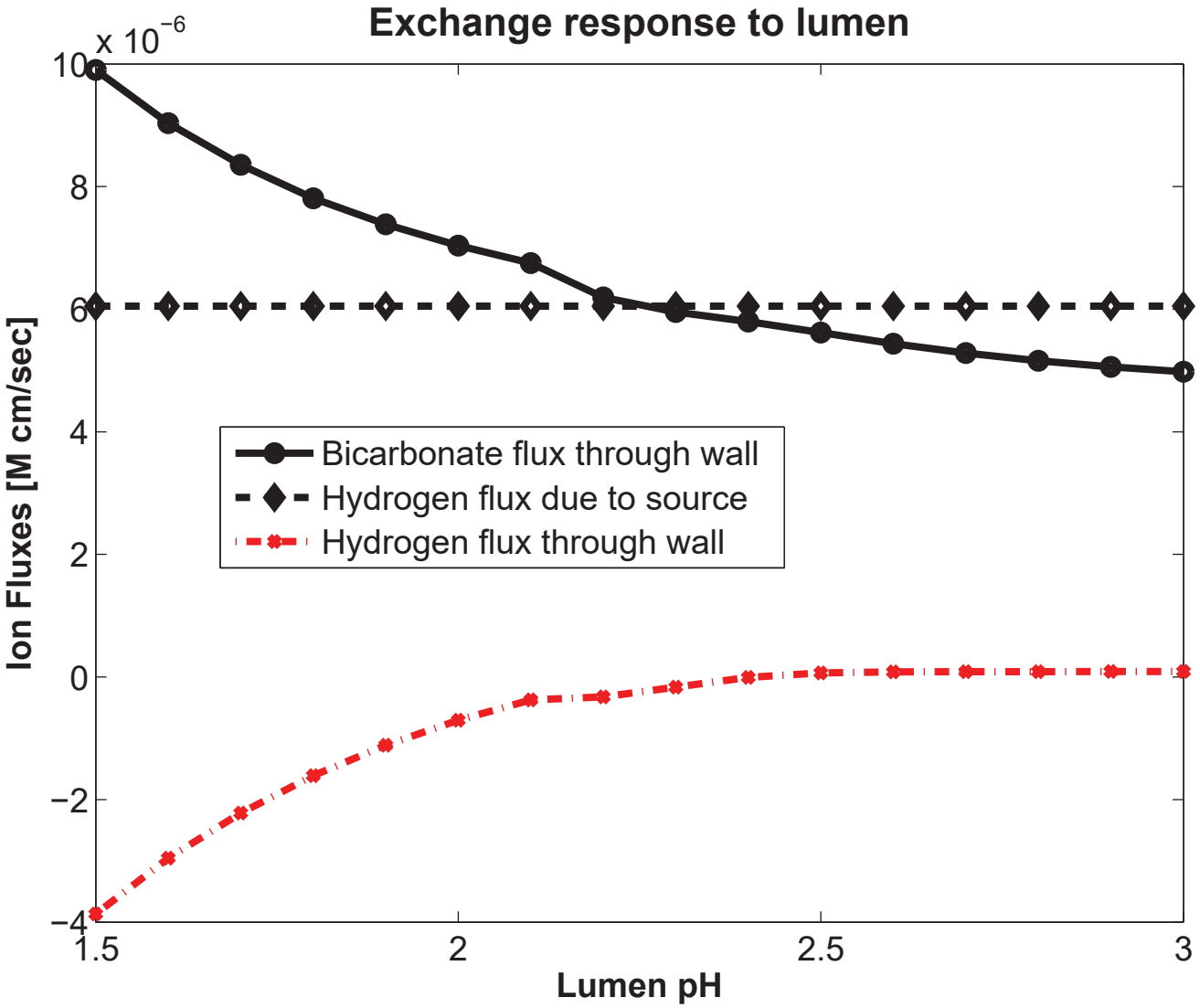
Exchange response to lumen
x 10^−6
10
8
6
4
2
0
−2
−4
1.5
2
2.5
3
Ion Fluxes [M cm/sec]
Lumen pH
Bicarbonate flux through wall
Hydrogen flux due to source
Hydrogen flux through wall

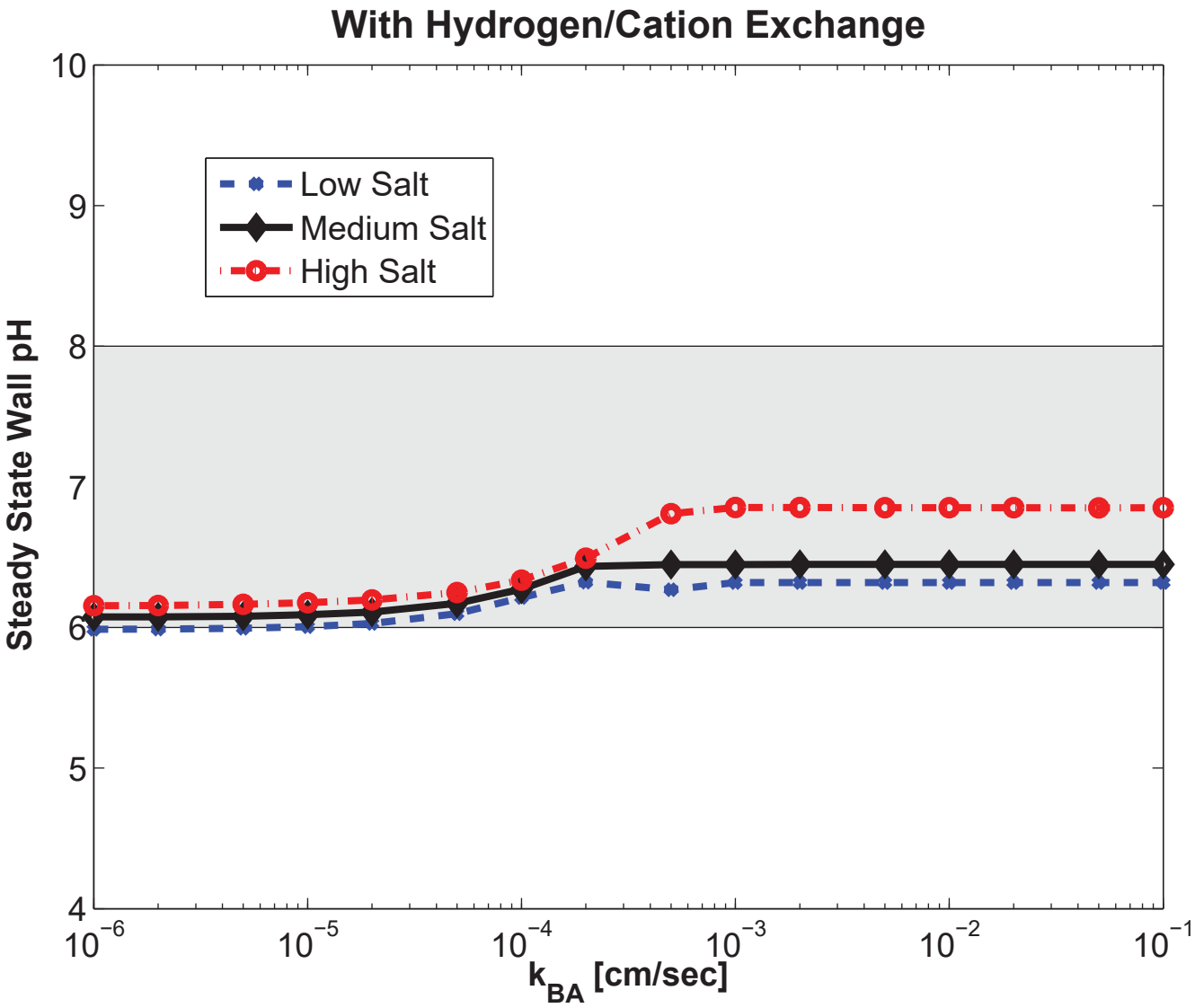
With Hydrogen/Cation Exchange
Low Salt
Medium Salt
High Salt
Steady State Wall pH
10
9
8
7
6
5
4
10^-6
10^-5
10^-4
10^-3
10^-2
10^-1
k_BA [cm/sec]

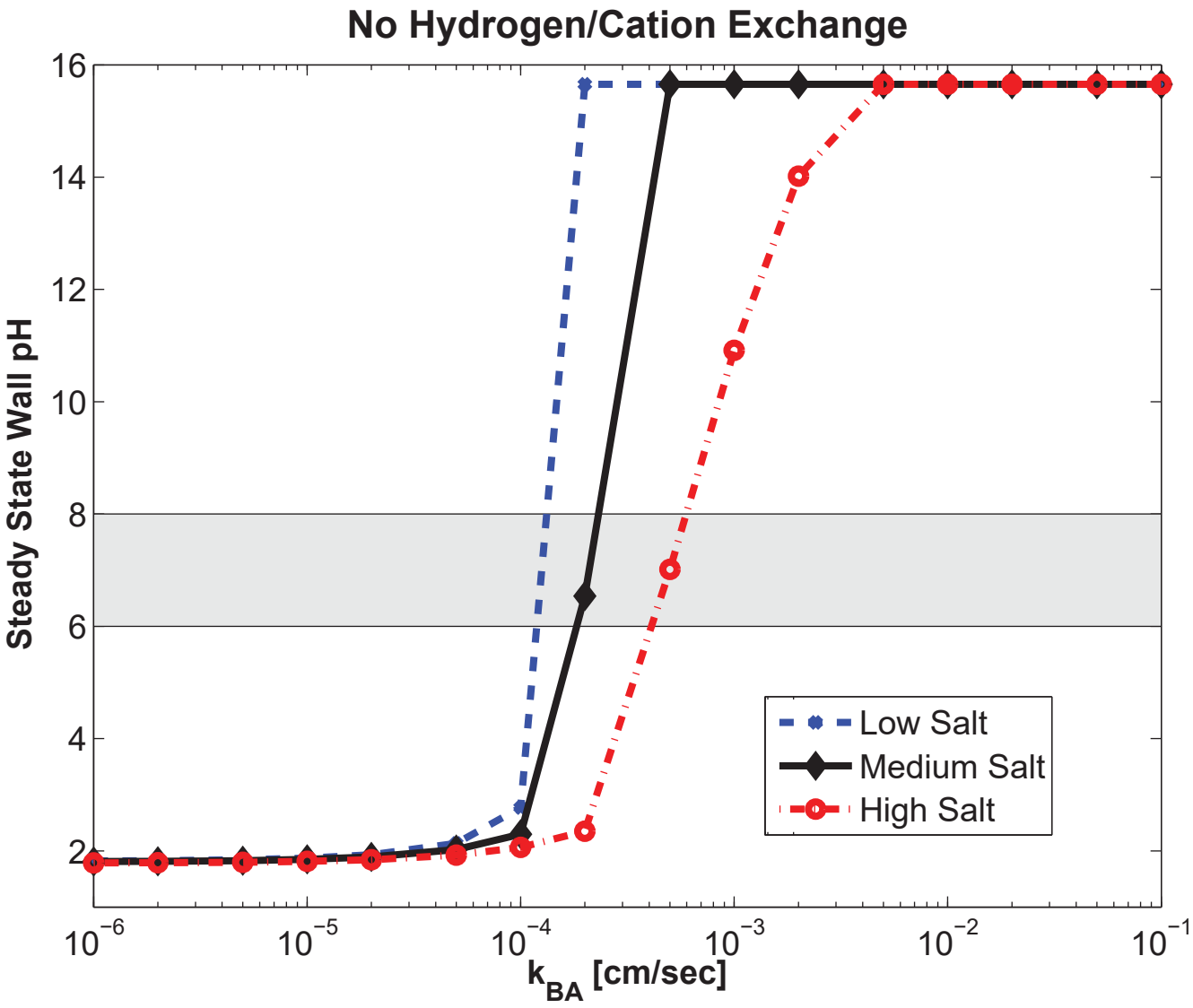
No Hydrogen/Cation Exchange
Steady State Wall pH
16
14
12
10
8
6
4
2
10^{-6}
10^{-5}
10^{-4}
10^{-3}
10^{-2}
10^{-1}
k_{BA} [cm/sec]
Low Salt
Medium Salt
High Salt

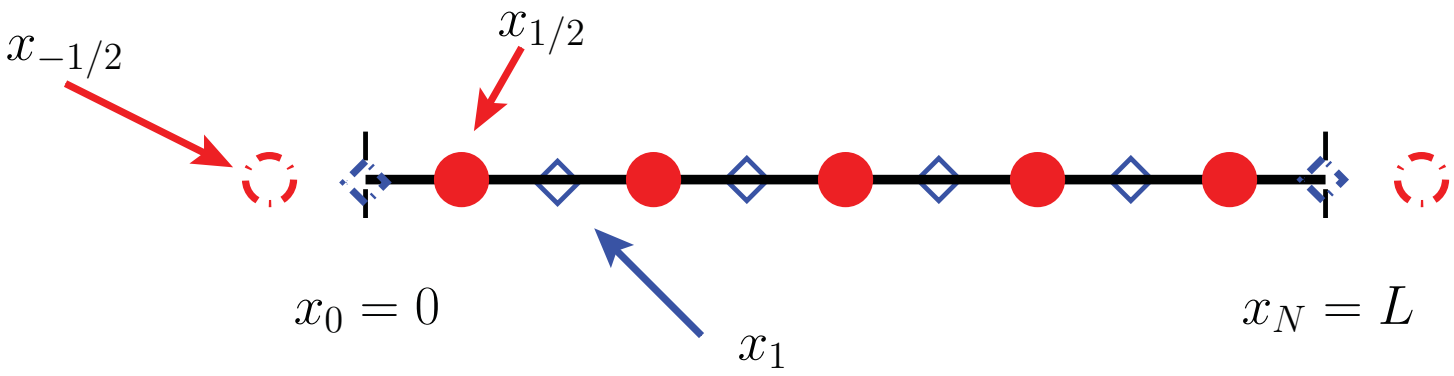
$x_{-1/2}$
$x_{1/2}$
$x_0 = 0$
x_1
$x_N = L$